Seasonal Oceanography from Physics to Micronekton in the South-West Pacific.

Menkes C.[a], Allain V.[b], Rodier M.[c], Gallois F.[d], Lebourges-Dhaussy A.[e], Hunt B. P. V.[f,g], Smeti H.[a,f], Pagano M.[f], Josse E.[e], Daroux A.[e], Lehodey P.[i], Senina I.[i], Kestenare E.[j], Lorrain A.[k], and S. Nicol[b]

[a] IRD (Institut de Recherche pour le Développement)-Sorbonne Universités (UPMC, Université Paris 06)-CNRS-MNHN, LOCEAN Laboratory, IRD Nouméa BP A5, 98848 Nouméa cedex, New Caledonia; christophe.menkes@ird.fr

[b] Secretariat of the Pacific Community, SPC, BP D5, 98848 Nouméa Cedex, New Caledonia; valeriea@spc.int, simonn@spc.int

[c] Institut de Recherche pour le Développement, IRD/UMR 241, IRD Tahiti, BP529, 98713 Papeete, Tahiti, French Polynesia; martine.rodier@ird.fr

[d] Institut de Recherche pour le Développement, IRD/US 199 IMAGO, IRD Nouméa BP A5, 98848 Nouméa cedex, New Caledonia; francis.gallois@ird.fr

[e] LEMAR/UMR6539, 29280 Plouzané, France ; Anne.Lebourges.Dhaussy@ird.fr, Erwan.Josse@ird.fr, aurelie.daroux@hotmail.fr

[f] Mediterranean Institute of Oceanography, MIO, UM 110, Aix Marseille Université, CNRS, Université de Toulon, IRD, MIO UM 110, 13288, Marseille, France. bhunt@eos.ubc.ca, houssem.smeti@gmail.com, marc.pagano@ird.fr

[g] Department of Earth Ocean and Atmospheric Sciences, University of British Columbia, Vancouver, BC, V6T1Z4, Canada

[h] National Institute of Marine Sciences INSTM. 28 rue 2 mars 1934, Salammbô, Tunisia

[i] CLS, 31520 Ramonville, France; plehodey@cls.fr, inna.senina@gmail.com

[j] Institut de Recherche pour le Développement, IRD/ UMR-LEGOS-OMP 5566, 31400 Toulouse, France; Elodie.kestenare@ird.fr

[k] Institut de Recherche pour le Développement, IRD/ R195 LEMAR, IRD Nouméa, BP A5, 98848 Nouméa cedex, New Caledonia; anne.lorrain@ird.fr

Re-Submitted to Deep Sea Research II CLIOTOP special issue. 28/05/2014

Corresponding author: Christophe Menkes christophe.menkes@ird.fr, phone: +(687) 261000

Abstract

Tuna catches represent a major economic and food source in the Pacific Ocean, yet are highly variable. This variability in tuna catches remains poorly explained. The relationships between the distributions of tuna and their forage (micronekton) have been mostly derived from model estimates. Observations of micronekton and other mid-trophic level organisms, and their link to regional oceanography, however are scarce and constitute an important gap in our knowledge and understanding of the dynamics of pelagic ecosystems. To fill this gap, we conducted two multidisciplinary cruises (Nectalis1 and Nectalis2) in the New Caledonian Exclusive Economic Zone (EEZ) at the southeastern edge the Coral Sea, in 2011 to characterize the oceanography of the region during the cool (August) and the hot (December) seasons. The physical and biological environments were described by hydrology, nutrients and phytoplankton size structure and biomass. Zooplankton biomass was estimated from net sampling and acoustics and micronecton was estimated from net sampling, the SEAPODYM ecosystem model, a dedicated echosounder and non-dedicated acoustics. Results demonstrated that New Caledonia is located in an oligotrophic area characterized by low nutrient and low primary production which is dominated by a high percentage of picoplankton cyanobacteria *Prochlorococcus* (>90%). The area is characterized by a large-scale north-south temperature and salinity gradient. The northern area is influenced by the equatorial Warm Pool and the South Pacific Convergence Zone and is characterized by higher temperature, lower salinity, lower primary production and micronekton biomass. The southern area is influenced by the Tasman Sea and is characterized by cooler temperature, higher salinity, higher primary production and micronekton biomass. Interactions between the dynamic oceanography and the complex topography creates a myriad of mesoscale eddies, inducing patchy structures in the frontal area. During the cool season, a tight coupling existed between the ocean dynamics and primary production, while there was a stronger decoupling during the hot season. There was little difference in the composition of mid-trophic level organisms (zooplankton and micronekton) between the two seasons. This may be due to different turn-over times and delays in the transmission of primary production to upper trophic levels. Examination of various sampling gears for zooplankton and micronekton showed that net biomass

estimates and acoustic-derived estimates compared reasonably well. Estimates of micronekton from net observations and the SEAPODYM model were in the same range. The non-dedicated acoustics adequately reproduced trends observed in zooplankton from nets, but the acoustics could not differentiate between zooplankton and micronekton and absolute biomasses could not be calculated. Understanding the impact of mesoscale features on higher trophic levels will require further investigation and patchiness induced by eddies raises the question of how to best sample highly dynamic areas via sea experiments.

Keywords

Zooplankton, nekton, acoustic data, oceanographic surveys, mesoscale eddies, oligotrophic, primary production

1 Introduction

In the South Pacific Ocean fishing of apex predators, such as tuna and billfishes, represents a major economic and food resource (Bell et al., 2013). Considerable variability in tuna catch rates is observed in fisheries (Rouyer et al., 2008). Although much of this variability remains unexplained, tuna abundance in space and time has been correlated with factors including oceanographic conditions, physiological constraints (*e.g.* temperature, depth, oxygen requirements), forage availability, and reproductive behavior (Farley et al., 2013; Senina et al., 2008; Young et al., 2011).

Tuna forage predominantly comprises micronekton (Young et al., 2010; this issue). Micronekton are defined as organisms in the 2-20 cm size range and are predominantly distributed in the upper 1000 m of the water column. Micronekton play a key role as intermediaries between plankton production, their prey, and top predators. Since micronekton biomass is dependent on the availability of plankton prey, it is expected that plankton production, its oceanographic drivers, and micronekton biomass would be tightly coupled, and therefore act in concert in determining top predator distributions.

The New Caledonian Exclusive Economic Zone (EEZ), a region of more than 1.4 10^6 km², is located in the Coral Sea, at the southeastern edge of the South Pacific (Figure 1). The dominant feature of circulation across 0-150 m is the westward-flowing South Equatorial Current (SEC) from ~25°S to the equator. The SEC flow bifurcates at the Australian continental margin (Ridgway and Dunn, 2003) at ~15°S, with one branch connecting with the southward flowing East Australian Current (EAC) (Qu and Lindstrom, 2002) and the other forming the Gulf of Papua Current which flows northward along the coast of Queensland. Within the Coral Sea, the SEC comprises narrow filaments and jets created by the complex island, reef, seamounts and ridge topography (Gourdeau et al., 2008) namely the North Vanuatu Jet at around 13-15°S, and the North Caledonian Jet at around 17-18°S (Couvelard et al., 2008; Marchesiello et al., 2010). To the south of New Caledonia, the surface flow returns from the EAC back into the central south Pacific (Figure 1) as the South Tropical Counter Current (STCC) (Marchesiello et al., 2010). In this region, the structures of the ocean currents are prone to shear instabilities and high eddy kinetic energy is observed

(Qiu et al., 2009). Excluding the very coastal areas, the New Caledonian EEZ is regarded as oligotrophic (Dandonneau and Gohin, 1984) with a mean nitracline depth of ~110 m (Figure 1). South of 22°S, the region experiences higher productivity (Ceccarelli et al., 2013; Dandonneau and Gohin, 1984).

Within this oceanographic context, the longline fishery for tuna represents approximately 30% of the total fisheries harvest in New Caledonia (Gillett, 2009). Catches are dominated by albacore tuna (*Thunnus alalunga*) and exhibit two seasonal peaks in July - August and December, and the highest catch rates occur in the north-western part of the EEZ (Briand et al., 2011). The influence of temperature, primary production and micronekton density on tuna catch rates has been demonstrated in New Caledonia (Briand et al., 2011), in American Samoa (Domokos, 2009) and at the ocean basin scale in the Pacific Ocean (Lehodey et al., 1998).

Large-scale observations of temperature, surface currents and surface primary production derived from satellite data have allowed validation of the existing oceanographic models, giving confidence in the use of modeled oceanographic parameters for such analyses. However there are few observations of biological parameters, including micronekton, to validate the model biological outputs.

At the scale of the South Pacific, nutrient and *in situ* phytoplankton data are sparse, as are data on zooplankton (Carassou et al., 2010; Le Borgne et al., 2011; McKinnon, 2005; Young et al., 2011). Knowledge of the micronektonic communities and their distributions is somewhat more comprehensive, but is based primarily on top predator diet studies (Allain et al., 2012; Olson et al., 2014; Young et al., 2011, 2010). Few data are available from *in situ* sampling with nets in the South Pacific (Flynn and Paxton, 2012; McPherson, 1991) and in general, none of the available micronekton data are coupled with information on oceanographic conditions. These constitute important gaps in our knowledge and understanding of the dynamics of the pelagic ecosystem.

Prior to this study, *in situ* data on micronekton in the New Caledonian region were derived from a handful of studies conducted in the eastern part of the EEZ (Grandperrin, 1975,

1969; Legand et al., 1970; Roger, 1986, 1974). Overall, data from the New Caledonia region are limited in both space and time, prohibiting a comprehensive description of the pelagic ecosystem, including the main seasonal patterns of zooplankton and micronekton and their relationships with the oceanography.

In 2011, we conducted two dedicated multi-disciplinary bio-oceanographic cruises (Nectalis1 and Nectalis2) in an effort to fill some knowledge gaps highlighted above for the New Caledonian and greater South Pacific region. Oceanography, nutrient and food web components were sampled in areas of high (north-west) and low (north-east) albacore tuna catch rates in the New Caledonia EEZ, during the austral cool and hot seasons when oceanography is contrasted and tuna catches high. The primary aim of these cruises was to provide insights into how phytoplankton, zooplankton and micronekton are coupled with ocean dynamics in the upper water column (0-1000 m). Here we describe the overall structure of the food web using *in situ* measurements of hydrodynamic parameters, nutrients, phytoplankton distribution, primary production, and the biomass of zooplankton and micronekton. We pay particular attention to the inter-comparability of the zooplankton and micronekton sampling techniques (nets and acoustics) used, and the application of acoustic techniques to improve estimates of micronekton in the future. We also use the collected data to assess measures of micronekton estimated using the ecosystem model SEAPODYM (Lehodey et al., 2010). Finally we interpret our findings in the context of the broader southwest Pacific.

2 Methods and data

Two scientific cruises, Nectalis 1 and 2 were conducted onboard the R/V Alis from 29 July to 16 August 2011 (austral cool season - 18 sampling stations) and 26 November to 14 December 2011 (austral hot season - 23 sampling stations) within the New Caledonian EEZ (Figure 2 and 3). The two cruises were conducted on approximately the same track, with some differences due to weather conditions. The potential spatial variability introduced by variability in station positions between cruises was considered minimal in view of the

variability of this highly dynamic pelagic system. Details of station sampling and continuous measurements are summarized in Table 1 and detailed below. Comparisons of ensuing data made between cruises included all stations.

2.1 Data collected during the cruises

2.1.1 **S-ADCP currents**

Five minute averaged ocean currents were acquired from 8 m bins across 16 to 200 m depth using a ship-borne 153 kHz Acoustic Doppler Current Profiler (ADCP – Teledyne RD Instrument, Seattle, USA). These velocity profiles were edited and processed using the CODAS software, (http://currents.soest.hawaii.edu/docs/adcp_doc/codas_setup/index.html) following the procedure of Hummon and Firing (2003). Data presented are averages over the top 150 m.

2.1.2 **Temperature and salinity**

An on-board thermosalinograph continuously measured sea surface temperature (SST) and salinity (SSS). At each station, Conductivity Temperature Depth (CTD) casts down to 500 m recorded continuous vertical profiles of temperature and salinity. CTD data were checked for spurious values using the Seasoft software (Sea-Bird electronics, Washington, USA), binned at 1m intervals and presented for the top 200 m.

2.1.3 **Water sampling**

Water was sampled during the CTD casts using 8 L Niskin bottles to measure nutrients, chlorophyll, phytoplankton cell counts, photosynthetic pigments and primary production. Depth and frequency of sampling varied according to variables measured and associated analyses (Table 1).

2.1.4 **Nutrients**

Nitrate, phosphate (Soluble Reactive Phosphorus: SRP) levels were measured in $HgCl_2$-poisoned samples and analyzed in the laboratory within two months of the end of the cruises using an Auto-analyzer AA3 (Bran+Luebbe, Norderstedt, Germany), as described in Aminot and Kérouel (2007). Nitrate and nitrite (reported as NO_3) concentrations were determined at nanomolar precision (Raimbault et al., 1990). SRP concentrations (reported

as PO_4) were analyzed according to Murphy and Riley (1962). Data were interpolated to plot the 0-180 m vertical profiles using Dr Masson's SAXO package (http://forge.ipsl.jussieu.fr/saxo/download/xmldoc/whatissaxo.html) based on IDL (Interactive Data Langage, Exelisvis, Boulder, USA).

2.1.5 **Phytoplankton: biomass and community structure**

Phytoplankton composition and community structure were identified from water samples collected (Table 1) and results were averaged across the depths: 0-50 m and 50-130 m.

2.1.5.1 Chlorophyll

In situ chlorophyll a (Chl-a) values were determined after methanol extraction (Le Bouteiller et al., 1992), using a Turner Design fluorometer (Turner Designs, Sunnyvale, California, USA, module # 7200-040, Chl-a extracted-acidification) calibrated with pure Chl-a standard (Sigma). Total Chl-a concentrations were determined from 0.5 L water samples filtered onto GF/F Whatman filters. Size-fractioned Chl-a across the size classes <3 µm, 3-10 µm and >10 µm was determined from 2 L water samples collected onto 10 µm, 3 µm nucleopore and GF/F filters by in-line serial filtrations, and represented proxies of pico-, nano and microphytoplankton biomasses respectively. The mean and standard deviation of size-fractionated Chl-a percentages were calculated for each cruise. Total Chl-a data were interpolated to plot the 0-150 m vertical sections of each cruise using the SAXO package.

2.1.5.2 *Cell counts by flow cytometry (FCM)*

Water samples of 1.1 mL were fixed by adding paraformaldehyde solution (2% final concentration) and then frozen in liquid nitrogen on board. Cell counts for pico and nanophytoplankton (<3 µm, 3-10 µm respectively) were performed with a FACSCalibur flow cytometer (BD Biosciences, San Jose, California, USA) at the Regional Flow Cytometry Platform for Microbiology (PRECYM) (http://precym.com.univ-mrs.fr). Data were normalized using both Fluoresbrite® Fluorescent Microspheres (Polysciences Inc. Europe) and TruCountTM beads (BD) and the mean and standard deviation of cell count percentages were calculated for each cruise.

2.1.5.3 Phycoerythrin

Water samples (4.5 L) were filtered onto 0.4 µm Nucleopore polycarbonate membrane filters (47 mm diameter) and immediately frozen in liquid nitrogen until analysis. Using methods described in Neveux et al. (2009), phycoerythrin (PE) was extracted in a 4 mL glycerol-phosphate mixture (50/50) after vigorous shaking for resuspension of particles (Wyman, 1992). Using a Perkin Elmer LS55 spectrofluorometer (PerkinElmer, Inc., Waltham, Massachusetts, USA) and emission and excitation slit widths adjusted to 5 and 10 nm, respectively, the PE fluorescence excitation spectra were recorded between 450 and 580 nm (emission fixed at 605 nm). Quantitative estimates of phycoerythrin were obtained from the area below the fluorescence excitation curve, after filter blank subtraction and the mean and standard deviation calculated for each cruise.

2.1.6 **Primary production**

Net primary production (NPP, mgC m^{-3} d^{-1}, Table 1) was measured using the ^{14}C tracer technique (RochelleNewall et al., 2008). Water samples (76 mL) were inoculated with 0.40 MBq of a sodium ^{14}C bicarbonate solution (Perkin Elmer, initial concentration 37 MBq mL^{-1}) and immediately placed in a thermoregulated (22-24°C) photosynthetron to incubate samples at varying light levels (11%, 28%, 48%, 68%, 100%). After 1.5 h incubation, samples were filtered onto 0.4 µm polycarbonate filters (25 mm Whatman Cyclopore) which were then placed into clean glass liquid scintillation counting vials and stored at -20 °C. In the laboratory, 100 µL of 0.5N HCl was added to each sample, and the vial left open for 12 h under a fume hood to remove unfixed ^{14}C. After acidification and drying, 5 mL of scintillation cocktail (Ultima Gold MV, Parkard instruments) was added to each sample, and the samples analyzed in a Packard Tri-Carb (1600TR) Liquid Scintillation Counter (PerkinElmer, Inc., Waltham, Massachusetts, USA). The mean and standard deviation were calculated for each cruise.

2.1.7 **Zooplankton**

Three methods were used to estimate zooplankton (organisms 2 µm – 20 mm) biomass: a Tracor Acoustic Profiling System (TAPS), net sampling and Ship-Borne Acoustic Doppler Current Profilers (S-ADCP).

246 *2.1.7.1 Tracor Acoustic Profiling System (TAPS)*

247 The TAPS-6™ (BAE systems, San Diego, CA, USA) is a six frequency (265, 420, 710, 1100,
248 1850, 3000 kHz) profiler (Holliday and Pieper, 1980) used to acoustically detect the micro-
249 (20-200 µm) and meso- (200-2000 µm) zooplankton from the surface down to 200 m. The
250 TAPS-6 was used in "cast mode", profiling the water column in horizontal position with a
251 descent speed of 0.5 m s^{-1}, sampling a volume of about 5 L of water at each ping (ping rate:
252 2.63 pings s^{-1}). The TAPS-6 focused on small and abundant organisms such as copepods,
253 with larger and less abundant organisms such as euphausiids having less chance to pass
254 through this small volume (Pieper et al., 2001).

255 The Scattering Volume (Sv) signal (in dB) was transformed into biovolume estimates using
256 an inversion algorithm following the method applied by Lebourges-Dhaussy et al. (2014) and
257 successfully applied to small zooplankton (e.g. Holliday et al., 1989; Lebourges-Dhaussy et
258 al., 2009; Napp et al., 1993; Pieper et al., 1990). The algorithm provided vectors of
259 abundances per size range for each station, from which biovolumes were estimated in
260 mm^3 m^{-3} and converted into mg m^{-3} using a density factor of ~1 kg L^{-1} (Simmonds and
261 MacLennan, 2005). The size range of organisms explored in the inversion process was 0.05-
262 3 mm (micro- and meso-zooplankton).

263 *2.1.7.2 Zooplankton net sampling*

264 Five layers of the water column were sampled from the surface down to 600 m depth (0-
265 100, 100-200, 200-400, 400-500, 500-600 m) using an Hydrobios MultiNet (Hydrobios, Kiel,
266 Germany). Each of the nets used were comprised of 200 µm nylon mesh and equipped with
267 a mechanical Hydrobios flowmeter. The volume filtered by each net was calculated using
268 the following equation:

269 $V=d*k*A$

270 where d is the number of revolutions of the flowmeter, k=0.3 m/revolution is the pitch of
271 the impeller of the flowmeter provided by the manufacturer (Hydro-Bios Apparatebau
272 GmbH, 2009) and A is the size of the net mouth area (0.25 m^2).

Samples collected by the nets were immediately preserved in a 5 % buffered formalin-seawater solution and processed for wet and dry weight analysis later in the laboratory. Dry weights (DW) and wet weights (WW) were determined for the 0-200 m and the 0-600 m layers respectively.

2.1.7.3 Ship-Borne Acoustic Doppler Current Profilers (S-ADCP) backscatter

The S-ADCP (see section 2.1.1), was also used to provide relative measures of acoustic density, as a proxy for zooplankton to micronekton biomass (Flagg and Smith, 1989; Heywood et al., 1991; Menkes et al., 2002; Radenac et al., 2010). At 153 kHz, this instrument roughly detects organisms across the size ranges of a few millimeters to a few centimeters (Sutor et al., 2005). The ADCP echo intensity (E_a) was converted into S_v (in dB) using the equation from Deines (1999) modified by Gostiaux and van Haren (2010):

$$Sv=C+10\log_{10}[(T_x+273.16)R^2]-L_{DBM}-P_{DBW}+2\alpha R+10\log_{10}[10^{KcEa/10}-10^{KcEnoise/10}]$$

where T_x is the temperature of the transducer (°C), L_{DBM} is $10\log_{10}$(transmit pulse, in meters), P_{DBW} is $10\log_{10}$(transmit power, in Watts), R is depth along the beam (m), α is the sound absorption coefficient (dB/m) in water, K_c is a conversion factor for echo intensity (dB/counts), E_a is the ADCP raw echo intensity (counts) and E_{noise} is the noise (counts). We used the default parameters given in Deines (1999) for the constants C and P_{DBW}. During the time that the ship was stationary at each station, when ship noise is reduced, we selected the minimum value of the echo intensities E_a in the vertical profiles and the minima were then averaged over the entire cruise to obtain E_{noise}.

2.1.8 **Micronekton**

Three methods were used to estimate micronekton (organisms 2 - 20 cm) biomass and species composition: using an EK60 echosounder, net sampling and the S-ADCP (see section 2.1.7.3).

2.1.8.1 EK 60 echosounder

Acoustic data were collected continuously during the cruise using a EK60 echosounder (SIMRAD Kongsberg Maritime AS, Horten, Norway) with four hull-mounted split-beam transducers (38, 70, 120 and 200 kHz). Echosounder calibration was performed according to

Foote et al. (1987) at the beginning of each cruise. Due to the presence of noise in echograms, linked to the specificities of the installation of the sounder on the R/V Alis and to rough seas during the cruises, the water column was only sampled down to depths of 100, 200, 250 and 600 m for the 200, 120, 70 and 38 kHz channels respectively. A data cleaning step was performed with Matlab® (MathWorks, Natick, Massachusetts, USA) filtering tools provided with the Movies3D software (IFREMER). The EK60 signal was analyzed in terms of scattering volume (Sv) (MacLennan et al., 2002). It was not possible to calculate micronekton biomass from echograms produced as the Sv to biomass conversion requires knowledge of the acoustic properties of the detected organisms added to a complex inversion of the signal and has not yet been performed for our dataset. The 38 kHz frequency is commonly used as a proxy for micronekton (Bertrand et al., 1999; Kloser et al., 2009; McClatchie and Dunford, 2003) and was used to represent micronekton over 0-600 m.

To describe the spatial structure of the micronekton biomass derived from the 38 kHz EK60, we removed the day/night signal from the data as the strong diurnal vertical migration of micronekton might mask spatial patterns. The data were assigned to either day or night and average values were calculated for each period for each cruise. The daytime (resp. nighttime) mean was subtracted from the daytime (resp. nighttime) values to produce anomalies for each period.

2.1.8.2 Micronekton net sampling

Micronekton were sampled at each station with a mid-water trawl with a 10 mm codend mesh size. Vertical and horizontal mouth opening of ~10 m each were monitored with trawl opening sensors (Scanmar, Åsgårdstrand, Norway). Horizontal tows were conducted to target aggregations visually detected with the EK60 echosounder. Once the trawl net was stabilised at the chosen depth, it was towed for 30 minutes at 3-4 knots. One or two tows were conducted at each sampling station between 14 and 130 m at night and between 21 and 540 m during the day. Organisms were sorted on-board into groups and frozen. In the laboratory, samples were identified at the lowest taxonomic level possible, counted, measured and weighed. Gelatinous organisms (e.g. siphonophores, salps, pyrosomes) were

329 weighed frozen as a group. Biomass was expressed as mg of wet weight per m^3 filtered. The
330 volume of water filtered by the net was calculated as:

331 V=S*D,

332 with S=h*v and D= R*c,

333 $c = 2 * \arctan(\sqrt{a/(1-a)})$

334 and $a=[\sin((lat_2-lat_1)/2)]^2 + \cos(lat_1)*\cos(lat_2)*[\sin((lon_2-lon_1)/2)]^2$

335 where V is the volume filtered (m^3), S is the net mouth opening (m^2), h and v are the net
336 horizontal and vertical mouth opening (m), D is the distance covered by the trawl (m),
337 $R=6371.e^{+3}$ m is the earth radius, lat_1, lat_2, lon_1, lon_2 are the latitude and longitude of the
338 start and the end of the set (radian).

339

340 ## *2.2 Other in situ, satellite and model derived datasets*

341 Estimated oceanographic and biological parameters derived from remote sensing and
342 physical and biological models were used to undertake direct comparisons between *in situ*
343 data and satellite and model derived parameter estimates and investigate relationships of in
344 situ data collected during each cruise with broader scale regional ocean dynamics .

345 ### 2.2.1 **Ocean Currents**

346 We used two datasets, the Kessler and Cravatte (2013) *in situ* dataset and the Ocean
347 Surface Current Analysis (OSCAR, http://www.oscar.noaa.gov/) satellite-derived dataset.
348 The first describes the time-averaged total geostrophic circulation of the top 1000 m. The
349 second provides surface currents estimated from a combination of data derived from
350 drifting buoys and altimetry at a 5-day and $1/3^o$ resolution.

351 ### 2.2.2 **Eddies: Okubo-Weiß parameter**

352 Surface ocean dynamics were examined using an eddy detection algorithm. The Okubo-
353 Weiß (OKW) parameter was calculated from the OSCAR surface currents. It describes the

354 deformation (shear and strain) and rotation (vorticity) of surface currents (Chelton et al.,
355 2011b; d' Ovidio et al., 2013; Dutrieux et al., 2008). This parameter allows discrimination of
356 regions where fluids circulate in a closed loop (OKW < 0, e.g. in the interior of eddies where
357 vorticity is high) from regions where shear and strain are high (OKW > 0, e.g. on the edges of
358 eddies where strain is high). The OKW parameter is always negative within vortices whether
359 they are cyclonic or anticyclonic (Chelton et al., 2011b).

360 2.2.3 **Sea Level Anomaly (SLA)**

361 Sea level anomalies (relative to the long term mean across the period 1993-2010) were
362 extracted from http://www.aviso.oceanobs.com/en/data/products/sea-surface-height-
363 products/global/msla.html#c5122 at a resolution of 1/3° and 7 days. SLA was used to
364 identify downwelling (high values or ridges in SLA) versus upwelling eddies (low values or
365 troughs in SLA).

366 2.2.4 **Sea Surface Temperature (SST)**

367 Daily SSTs from the Group for High Resolution SST (GHRSST) were downloaded from the
368 website https://www.ghrsst.org/ and used to examine spatial patterns in SSTs in the New
369 Caledonian EEZ. This freely available product combines several satellite data sources and is
370 provided at 1/12° grid resolution.

371 2.2.5 **Primary production**

372 Depth-integrated primary production was estimated from satellite-derived chlorophyll,
373 Photosynthetically Available Radiation (PAR) fields and SST fields using the Vertically
374 Generalized Production Model (VGPM) (Behrenfeld and Falkowski, 1997). Primary
375 production was integrated across the euphotic layer, which was statistically derived from
376 satellite imagery (http://www.science.oregonstate.edu/ocean.productivity/). Satellite-
377 derived chlorophyll is calculated from ocean color data, which, for the period 2002-2009,
378 were derived from the Sea-viewing Wide Field Of View Sensor (SeaWiFS) satellite after
379 which data were computed at CLS (www.cls.fr) using the VGPM model and Moderate
380 Resolution Imaging Spectroradiometer (MODIS) and Medium Resolution Imaging
381 Spectrometer (MERIS) satellite data. PAR data were derived from the European Center for
382 Medium Range Forecast (ECMWF) analyses.

2.2.6 **Micronekton from the SEAPODYM model**

The end-to end spatial ecosystem model SEAPODYM (Lehodey et al., 2008) describes the interactions of tuna species with the environment and incorporates external forcings associated with fishing and the environment. It includes environmental parameters such as temperature, currents, oxygen and primary production as well as a micronekton sub-model describing the transfer of energy from primary production to tuna species through mid-trophic levels. The sub-model comprises six functional groups of micronekton occupying different water layers according to day and night (diel migration model). Modelled micronekton is advected by currents and assimilates carbon from primary production produced three months earlier (Lehodey et al., 2010).

The micronekton sub-model is driven by satellite-derived primary production (see section 2.2.5) and by the outputs of the GLobal Ocean ReanalYsis and Simulations (GLORYS2.V1) of currents and temperature produced by the French Groupe Mission Mercator Coriolis (Barnier et al., 2006; Ferry et al., 2012) across two reanalysis periods 2002 – 2008 and 2009 - 2012. The 2002 – 2008 reanalysis was conducted at a daily and 1/4° resolution and was performed by the MERCATOR-OCEAN operational oceanography center. It is forced by daily surface meteorological data from the European Centre for Medium-Range Weather Forecasts (ECMWF). By assimilating satellite-derived sea level anomalies, sea surface temperatures and *in situ* measurements of vertical temperature and salinity profiles, the model estimates realistic mesoscale activity with eddy field variability in good agreement with altimetric data. Reanalysis across 2009-2012 included temperature and currents provided by the same numerical ocean model, while altimetry, SST and temperature/salinity profiles were also assimilated in their operational configuration (http://www.mercator-ocean.fr/)(Abecassis et al., 2013).

The biomass distribution of micronekton functional groups along the cruise track and in the south-west Pacific at the time of the cruises was estimated with the SEAPODYM ecosystem model using a revised definition of vertical biological layer boundaries, at a spatial resolution of 1/4° averaged over 7 days. Vertical biological layers comprised the epipelagic layer, which lies between the surface and the euphotic depth (derived from ocean color

satellite data and the VGPM model), the mesopelagic layer located at 1-3 times the euphotic depth, and the bathypelagic layer located at 3-7 times the euphotic depth. The model simulates a diel behavior of micronekton by considering that during the night, daily migratory species can move from one layer to another, thus adding to the residing biomass of non-migratory species of the layer. Because we used 7-day outputs to compare with the continuous Nectalis data, we reconstructed a SEAPODYM time series with a day/night signal that mimicked the Nectalis data. We interpolated the Nectalis tracks into the SEAPODYM model. This interpolation was temporally referenced so that day and night estimates from SEAPODYM could be extracted.

To describe the spatial structure of the micronekton biomass derived from SEAPODYM, we removed the day/night signal from the data by calculating anomalies following the same procedure than for 38 kHz EK60 (see section 2.1.8.1).

2.3 Statistics and comparison of methods

2.3.1 **Primary production**

The non-parametric rank-sum Wilcoxon-Mann-Whitney test at α=5% was used to test the seasonal difference in *in situ* primary production values and in VGPM satellite-derived primary production along the cruise track. Spatial auto-correlation was eliminated from the VGPM dataset by building a new dataset of independent points before conducting the seasonal comparison.

To build this new dataset of independent points, we determined the distance ("d" in km) at which two points are independent. The initial auto-correlated dataset was then resampled selecting a point every "d" kilometers creating a dataset of independent points. Shifting the start position of this subsampling by 1 km, another dataset of independent points was then created. This procedure was repeated until the number of resampled datasets of independent points was equal to "d", and contained a number "n" of independent points which was the length of the cruise track divided by "d". In the statistical tests the "d" resampled datasets of independent points were all tested and the result of the test

(difference or no difference) comes with the percentage of the number of "d" tests producing this result.

To estimate the distance "d" between two independent points, empirical spatial variograms with 10km bins were used. The variogram of the VGPM dataset was compared to the noise constructed from a series of variograms of 100 randomly re-ordered VGPM datasets by a Monte Carlo procedure. The distance "d" at which the dataset points become uncorrelated was estimated when the variogram of the dataset reached the noise.

For the VGPM dataset "d" was estimated at ~50 km during Nectalis1 and 100 km during Nectalis2. Overall a conservative value of 100 km between two successive data points was considered, prompting ~ 100 possible VGPM datasets of 30 independent points (or, equivalently degrees of freedom) for Nectalis1 and 35 independent points for Nectalis2. These 100-ensemble datasets were used for seasonal comparisons.

We estimated that *in situ* primary production points were independent (no spatial auto-correlation) on the basis that the minimum distance between two sampling stations where *in situ* primary production was measured (144 km) is greater than the estimate at which 2 points were determined to be independent using the VGPM dataset (100 km).

The Wilcoxon-Mann-Whitney test at α=5% was also used to compare *in situ* primary production to VGPM data at the location of the *in situ* measures (12 data points). For small sample sizes, values for significance were read in classical tables, while where sample sizes were n>20 degree of freedom, the test was calculated using IDL's routines (imsl_wilcoxon.pro).

2.3.2 **Zooplankton**

A Wilcoxon-Mann-Whitney test at α=5% was used to test for seasonal difference in zooplankton biomasses estimated from the zooplankton net (in DW and WW), the TAPS and the S-ADCP backscatter. We accounted for the spatial auto-correlation of the S-ADCP by following the procedure described in section 2.3.1. For the S-ADCP dataset, the distance "d" at which two points were considered independent was 30 km for both cruises. Consequently, 30 datasets of 100 and 116 independent points were built for Nectalis1 and

Nectalis2 respectively for statistical analyses. We estimated that *in situ* zooplankton biomass estimates (zooplankton net and TAPS) points were independent (no spatial auto-correlation) on the basis that the minimum distance between two sampling stations (67 km) is greater than "d" (30 km).

The potential for the S-ADCP to provide a proxy of zooplankton biomass was evaluated against the log-transformed biomass measurements of zooplankton derived from the TAPS and net sampling using a Spearman's correlation.

For this general overview, no detailed examination of zooplankton spatial distribution and composition were conducted, but will be conducted in a separate study (Smeti pers. comm.).

2.3.3 **Micronekton**

A Wilcoxon-Mann-Whitney test at α=5% was used to test for seasonal differences in micronekton biomass estimated by the EK60 and by the SEAPODYM ecosystem model. No seasonal comparison was conducted on net sampling because of differences in sampling strategies between the two cruises (non-comparable depth or day-night tows). We accounted for the spatial auto-correlation of the 38 kHz EK60 Sv and SEAPODYM micronekton biomass estimates by following the procedure described in section 2.3.1. For the 38 kHz EK60 Sv dataset the distance "d" at which two points were considered independent was 30 km for both cruises. Consequently, 30 datasets of 100 and 116 independent points were built for Nectalis1 and Nectalis2 respectively for statistical analyses. For the SEAPODYM dataset, "d" was estimated at 100 km for Nectalis1 and 50 km for Nectalis2. A conservative value of "d"=100 km was used for both cruises to build 100 datasets of 30 and 35 independent points for Nectalis1 and Nectalis2 respectively.

The potential for the S-ADCP to provide a proxy of micronekton biomass was evaluated against the Sv values of the four frequencies of the EK60 echosounder. To do this, the EK60 high-resolution time and vertical profiles were averaged to the ADCP time/vertical resolution. The Sv was calculated for a 5-minute Elementary Sampling Unit (ESU) and 8 m height layers. Correlations between data provided by the S-ADCP and the four frequencies

of the EK60 were investigated using a Spearman's correlation. We accounted for the spatial auto-correlation by computing 30 correlation coefficients from the 30 resampled datasets of independent points distant of 30 km, as explained above. The range of correlation coefficients from the 30 correlation ensemble was provided as well as the percentage of these correlations significant at α=5% level.

Estimates of epi and mesopelagic micronekton biomass (mg m^{-3}) derived from SEAPODYM were compared to the estimates of micronekton biomass derived from the 38 kHz EK60 echosounder. The high-resolution EK60 data were averaged across ¼ degree grid squares along the cruise track to correspond with the spatial resolution of the SEAPODYM ecosystem model. Correlation between the two data series was investigated applying the same procedure as for EK60 *vs.* S-ADCP. and accounting for the Spatial auto-correlation was accounted for by calculating the correlation on 100 resampled datasets of independent points distant of 100 km from the two biomass series..

3 Results

3.1 Physical oceanography and biogeochemistry

3.1.1 **Surface features**

During the cool season (Nectalis1) thermosalinograph measurements showed that surface waters in the southern part of the cruise track (south of 19°S) had an average temperature of 23.6 ± 1.0 °C and salinity of 35.2 ± 0.2 while the northern part of the cruise was characterized by waters of 25.3 ± 0.7°C and 35.0 ± 0.1 (Figure 2). During the hot season (Nectalis2), overall SST and SSS patterns were similar, although temperatures were warmer by ~3°C. Salinity was very similar in the south but lower by ~0.1 in the north (Figure 3). During both cruises, salinity varied across similar gradients to temperature, but in the opposite direction at both larger-scales and smaller scales. For example, high temperature and low salinity waters were observed during Nectalis1 at stations 4 and 5 with waters with

522 particularly low temperature and high salinity observed at stations 1 and 2 during both
523 cruises. This gradient was observed in particular during Nectalis2.

524 During both cruises, ADCP surface layer (0-150 m) currents varied in a similar way across
525 large and small spatial scales to surface-only currents derived from OSCAR. North of 19°S,
526 the currents were predominantly directed westward, while in the south they were
527 predominantly directed eastward. Along the western coast of the main island of New
528 Caledonia, currents were flowing predominantly south-eastward during Nectalis1 and
529 southward during Nectalis2. In addition to these broad scale patterns, high current
530 variability was observed, for example at stations 6-7 during Nectalis1 and stations 7-8-9
531 during Nectalis2.

532 Satellite-derived SST clearly showed the large-scale north-south gradient in observed during
533 both cruises. Smaller scale meandering of the SST field centered at ~19-20°S was observed
534 with strong association between the thermohaline patterns and the currents. Meanders
535 were noted through intrusions of warmer waters from the north which were advected
536 south (e.g. Nectalis1 station 8, 17, Nectalis2 station 9) and intrusions of cooler waters from
537 the south which were advected north (e.g. Nectalis1 stations 6, 7, 16, Nectalis2 stations 17-
538 18).

539 Values of OKW and SLAs along with current vectors from both OSCAR and S-ADCP described
540 an important turbulent eddy activity. Cyclonic eddies ("upwelling" type eddy) corresponding
541 to sea level depression (or equivalently, thermocline uplifting) were observed during the
542 cool season, for example at ~23°S 161°E (eddy A on Figure 2), at stations 6-7 (eddy B) and at
543 ~16.5°S 159°E (eddy C) the south-eastern edge of which was sampled at station 10 (Figure
544 2). During the hot season, strong cyclonic eddies were observed at ~24°S 156°E (eddy D on
545 Figure 3), ~24°S 164°E (eddy E) and ~25°S 172°E (eddy G) and a series of energetic eddies
546 were observed between stations 7 and 18 (eddies H, I, J). The edge and the center of an
547 anticyclonic eddy ("downwelling" type eddy with thermocline deepening and sea-level
548 ridge) were sampled during the hot season at stations 8 and 9 respectively (eddy K, Figure
549 3). Overall, lower eddy activity was observed during the cool season (Figure 2) than during
550 the hot season (Figure 3).

3.1.2 **Vertical structures**

During the cool season, stations 8 - 18 in the north and east were characterized by relatively warm, low salinity waters with a mixed layer depth of ~60m and low values of nitrate (0.05 ± 0.07 µM) to a depth of ~90 m (Figure 4). The Deep Chlorophyll Maxima (DCM) (~0.25-0.3 mg m^{-3}) and the nutricline were located at ~90 m depth (Figure 4). By contrast, stations 1 - 7 in the south and west were comparatively cooler with higher surface salinity. At these stations, higher concentrations of nitrate (0.13 ± 0.12 µM) and chlorophyll content occurred with more frequent maxima at the surface. Phosphate concentrations varied with an average of 0.067 ± 0.038 µM from the surface to 100 m depth and were occasionally lower than 0.05 µM in the surface layer. Within this general pattern, a number of stations demonstrated unique characteristics. Cool, highly saline waters which were homogeneous down to 100 m with a shallow nutricline and enhanced chlorophyll were recorded at stations 1 and 2 (Figure 4). Waters with a deep mixed layer, elevated chlorophyll from the surface down to 100 m were also recorded at stations 6 and 7, contrasting with the surrounding waters (Figure 4). High surface (0-20 m) chlorophyll levels (0.23 µg l^{-1}) were recorded at station 10 (Figure 4).

The north-south gradient in temperature and salinity observed during the cool season was also evident at depth during the hot season, with warmer and fresher waters north of ~20°S observed at stations 8 - 19 (Figures 3 and 4) and cooler and saltier waters south of ~20°S observed at stations 1 - 7 and 20 to 23 . The mixed layer across all stations was shallower during the hot season, located at ~25 m, denoting stronger surface stratification in the water column than during the cool season. Surface waters were low in nitrate (0.03 ± 0.02 µM) across almost the entire cruise track (Figure 4) and the DCM was often centered at around 100 m with mean values of ~0.41 ± 0.16 mg m^{-3}. In general, above the DCM in the top ~ 50 m, chlorophyll concentrations were slightly lower than during the cool season (Figure 4), particularly in the southern part of the survey area. Phosphate tended to be low (0.05 ± 0.03 µM) for stations 1 - 7 and 20 - 23 in the southern part of the cruise track in comparison to stations in the northern part of the cruise (0.09 ± 0.03 µM). A few stations had unusual characteristics: high temperatures and low salinities down to 100 m were

580 observed at station 9 and surface nitrate was slightly enhanced at stations 7 and 8
581 (0.09 ± 0.01 µM) compared to other stations (0.02 ± 0.02 µM).

582

583 ### *3.2 Primary production*

584 Depth- integrated measurements of *in situ* primary production in the photic layer and
585 similar satellite-derived net primary production (NPP) from VGPM along the cruise track
586 were significantly higher during the cool season (352±160 mgC m^{-2} d^{-1} and
587 301±62 mgC m^{-2} d^{-1} on average respectively) than during the hot season
588 (231±133 mgC m^{-2} d^{-1} and 199±55 mgC m^{-2} d^{-1}) (Figure 5 and Table 2)

589 The NPP pattern (Figure 2) demonstrated a strong gradient during the cool season with
590 values of ~350 mgC m^{-2} d^{-1} in the southern part of the survey area (south of 20°S and west
591 of the main island) and values lower than 200 mgC m^{-2} d^{-1} in the northern part of the survey
592 area (north of 20°S and east of the main island). During the hot season the entire region was
593 more oligotrophic, with a weaker north-south gradient, and average values of
594 ~200 mgC m^{-2} d^{-1} in the survey area (Figure 3). Within this large-scale gradient, specific
595 patterns linked to mesoscale structures were observed. For example, the center of some
596 eddies were characterized by enhanced primary production (e.g. Nectalis1 eddy A; Nectalis2
597 eddy D; Nectalis2 eddy G), while primary production was enhanced at the edge of others
598 (e.g. Nectalis1 station10 eddy C; Nectalis2 series of eddies H, I, J).

599 No significant differences were found between *in situ* production estimates and VGPM
600 satellite values at the *in situ* sample locations (Figure 5).

601

602 ### *3.3 Phytoplankton*

603 During the cool season, size fractionated chlorophyll was dominated by picophytoplankton
604 (< 3 µm) across all stations (mean=75.9% ± SD=17.2% in biomass); nano and micro-
605 phytoplankton represented 12.8% ± 9.6% and 11.3% ± 12.6% respectively of chlorophyll
606 biomass. The cyanobacteria *Prochlorococcus* were the dominant species of the

picophytoplankton group (91.9% ± 6.3% in abundance; Figure 4) with cell abundances of up to 250 x 10^3 mL^{-1}. Remaining abundances of picophytoplankton across stations were comprised of *Synechococcus* (6.3% ± 6.2%) and picoeukaryotes (1.8% ± 0.8%). Overall phytoplankton composition did not vary latitudinally or longitudinally, with the exception of particular features observed at stations 2 and 10 (eddy C). In comparison to other stations, higher proportions of large cells were observed at station 2 from the surface to 150 m (~30% nano- and ~28% microphytoplankton in abundance) and at station 10 from the surface to 50 m (~17% nano- and ~31% microphytoplankton in abundance).

The fractionated chlorophyll and community structure during the hot season was similar to that observed in the cool season with picophytoplankton and *Prochlorococcus* dominating the communities (83.4% ± 10.4% in biomass and 92.3% ± 7.8% in abundance respectively; Figure 4). Nano and micro-phytoplankton represented 8.6% ± 5.4% and 7.9% ± 7.1% respectively. However, cell abundance was much lower during the hot season, with maximum cell counts of *Prochlorococcus* of 160 x 10^3 mL^{-1}. Remaining cell abundances were comprised of *Synechococcus* (5.0% ± 6.8%) and picoeukaryotes (2.7% ± 1.7%). Again, the phytoplankton structure was relatively homogeneous along the cruise track with the exception of station 9 (eddy K) which had a higher proportion of larger cells from the surface to 50 m (~7% nano- and ~39% microphytoplankton in abundance) than the rest of the stations (~13% ± 3.1% nano- and ~11%±5.0% microphytoplankton in abundance; Figure 4). Phycoerythrin (PE) concentration was also much higher at this station (1836 fluorescence unit *vs.* 389 ± 359 fluorescence unit for the other stations).

3.4 Zooplankton

Diurnal variability in zooplankton biomass was observed with all methods, with enhanced biomass at night in the top 200 m during both cruises (Figure 6 and 7). Zooplankton WWs during the hot season however were relatively similar during the day and at night, which is at odds with dry weight (DW) estimates where diurnal variability is evident (Figure 6 and 7). Zooplankton wet weight (WW) (Figure 6) vertical profiles showed that the majority of the biomass concentrated in the top 100 m, deeper biomass rapidly decreased.

Mean biomass estimates from the TAPS (~ 100 mg m^{-3}) were more than one order of magnitude higher than WW estimates from net samples (< 6.5 mg m^{-3}) and DW estimates from net samples (< 6 mg m^{-3}) (Table 2). Zooplankton biomasses derived from TAPS and WW estimates across all sampling stations were not significantly different between the two cruises, while significant differences were observed in DW (Nectalis1<Nectalis2) and S-ADCP (Nectalis1>Nectalis2) estimates (Table 2).

Correlations between acoustic biomass proxies and net biomass measures for zooplankton were all significant, with the TAPS and S-ADCP having the highest correlation overall (Table 3). Estimates derived from net samples demonstrated similar correlations with those derived from the S-ADCP and those derived from the TAPS (Table 3). Correlation values between zooplankton measurements were roughly similar across the two depth ranges explored: 0-100 m and 0-200 m.

3.5 Micronekton

Preliminary examination of the micronekton composition indicated that micronekton net catch was dominated by gelatinous organisms (e.g. siphonophores, salps, pyrosomes), which represented 53.8% of the overall wet weight biomass. Fish, molluscs and crustaceans represented 36.5%, 7.6% and 2.1% of the biomass, respectively. In total, approximately 480 taxa were identified, including ~240 fish taxa, ~95 crustacean taxa, ~85 mollusc taxa and ~60 gelatinous organism taxa. Of those species able to be identified, those species with the highest biomasses in each taxa group were the lanternfish *Ceratoscopelus warmingii*, *Hygophum hygomii* and *Diaphus perspicillatus*; the molluscs *Sthenoteuthis oualaniensis, Abraliopsis sp.* and *Abralia omiae*; and the crustaceans *Thysanopoda tricuspidata, Thysanopoda cristata* and *Euphausia mucronata*. Of the gelatinous organisms the most abundant were Pyrosomatidae, Abylidae and *Pyrosoma atlanticum*.

Biomass estimates from *in situ* measurements from the micronekton nets for the 0-600 m and from SEAPODYM model were in the same range: ~ 4 mg m^{-3} (Table 2).

During both seasons, the EK60 and SEAPODYM signal anomalies indicated that the region north of ~19°S-20°S had lower micronekton biomass than the region south of this latitude (Figure 8). Smaller scale variability was also apparent in both datasets, most prominently south of 19°S-20°S where patches of higher biomass were observed; for example along the west coast of the main island and at ~20.5°S 161°E during Nectalis1 and ~20.5°S 158°E during Nectalis2.

Micronekton abundance estimated from the S-ADCP, the nets, the EK60 and the SEAPODYM model exhibited a clear maximum at night (Figure 7). Vertical profiles of the micronekton estimated from the 38 kHz EK60 Sv (Figure 6) demonstrated a bimodal distribution with higher micronekton biomass estimates occurring at 0-200 m and 400-600 m than at other depths during both the day and night.

Seasonal differences observed in micronekton biomass estimated by the EK60 Sv and SEAPODYM were not statistically significant (Table 2). Conversely, estimates derived from the S-ADCP were different with higher values during the cool season (Table 2).

Micronekton estimates derived from the EK60 Sv and S-ADCP Sv were highly correlated, and the highest correlation was observed with the 70 kHz EK60 (correlation range = 0.87-0.96) (Table 4). Micronekton biomass estimates calculated by the 38 kHz EK60 Sv were highly correlated with estimates derived from the SEAPODYM model (correlation range = 0.73-0.79) (Table 4).

4 Discussion

4.1 Oligotrophic waters and water masses

The physical, biogeochemical and biological data collected during the two Nectalis cruises, in two contrasting seasons, have provided new insights into the spatial and temporal dynamics of the pelagic ecosystem in the waters around New Caledonia. Observations collected from the two cruises support prior characterization of the region as oligotrophic. The vertical nutrient profiles, low nitrate and sometimes low phosphate, low primary

689 production and chlorophyll biomass, and a phytoplankton composition dominated by small
690 size cells (picophytoplankton), were consistent with previous studies in South Pacific region
691 (Campbell et al., 2005; Jacquet et al., 2006; Young et al., 2011) and are typical of a Low
692 Nutrient Low Chlorophyll (LNLC) system. Although it is generally thought that nitrate is the
693 main limiting nutrient in this oligotrophic region (Le Borgne et al., 2011), some
694 phytoplankton species may be limited by phosphate (Moutin et al., 2005) and this can
695 induce higher contributions of diazotrophs such as *Trichodesmium sp.* in this area.
696 *Trichodesmium sp.* was not observed in the samples we collected, but it was seen at the
697 surface of the water along the track at one occasion. Examination of isotope values
698 calculated from biological samples collected during the Nectalis cruises (Hunt et al., this
699 issue) suggests the contribution of diazotrophs to phytoplankton composition as previously
700 observed in the area (Campbell et al., 2005; Dupouy et al., 2011).

701 Two distinct water masses were encountered in the studied area. North of 19°S-20°S,
702 waters in the top 200 m were characterized by warm temperature, low salinity, low nitrate,
703 lower primary production and lower micronekton biomass estimates. These characteristics
704 are representative of the "Coral Sea" oligotrophic regime (Ceccarelli et al., 2013), and are
705 largely influenced by the warmer and fresher waters of the south Pacific convergence zone
706 (SPCZ) where the SEC predominantly flows,.

707 South of 19°S-20°S, waters are characterized by colder temperature, higher salinity, a
708 shallower nitracline, higher nitrate content in the surface layer, higher primary production
709 and higher micronekton biomass estimates and are under the influence of the South
710 Tropical Counter Current branches (Marchesiello et al., 2010).

711 Although water masses were variable latitudinally, phytoplankton compositions were very
712 similar throughout the whole area.

713 *4.2 Horizontal advection, mesoscale and submesoscale phenomena*

714 Large regional-scale organization of surface currents, SST, SSS and primary production was
715 observed to be strongly distorted by meanders and smaller scale phenomena under the
716 influence of horizontal advection from highly variable currents. The similarity of

717 temperature and salinity variations suggested the action of advection processes in
718 modifying salt and temperature at small scales. Numerous processes such as upwellings,
719 mesoscale (20-100 km, Lévy, 2008) eddies and submesoscale (2-20 km) fronts were
720 observed influencing the biological distributions in complex manners.

721 In the south/south-westward flowing the ALIS currents observed during the Nectalis cruises
722 along the west coast of New Caledonia (Marchesiello et al., 2010), an example of coastal
723 upwelling was observed at stations 1 and 2 during the two seasons. This coastal upwelling
724 was characterized by cool temperatures and high salinities observed to be homogeneous
725 down to 100 m during the cool season and down to 50 m during the hot season. During the
726 cool season the upwelling was also characterized by a shallow nutricline, enhanced
727 chlorophyll at the surface and higher proportion of large phytoplankton cells, which were
728 not observed during the hot season. A coastal upwelling induced by south-east trade winds
729 particularly during the hot season has been reported in a number of other studies
730 (Ganachaud et al., 2010; Marchesiello et al., 2010).

731 Observations during each season described quite turbulent ocean circulation with myriads
732 of small cyclonic and anticyclonic eddies of ~50-100 km in size. Such observations have also
733 been reported by Chelton et al. (2011b).

734 The region is known for its strong interactions between the SEC, which enters from the east,
735 the STCC flowing from the west and the tortuous topography of island masses and ocean
736 floor ridges. These interactions between the large scale currents and topography produce
737 non-linearities in the ocean currents (Couvelard et al., 2008; Marchesiello et al., 2010) which
738 can favor eddy developments. Eddies can also be associated with incoming Rossby waves
739 (Killworth et al., 2004) as well as barotropic instabilities resulting from the sheared
740 westward and eastward currents in the northern region of the EEZ (Figure 1). South of
741 ~22°S, Rossby waves and baroclinic instabilities between the surface flowing STCC and the
742 deeper flowing SEC are also known to generate eddy activity as depicted in strong ocean
743 eddy kinetic energy which peaks during the hot season (Qiu et al., 2009).

744 Primary production and phytoplankton composition within eddies can differ depending
745 upon the oceanographic processes and underlying trophic mechanisms operating in time
746 and space. At the mesoscale, cyclonic eddies (southern hemisphere) induces upwellings
747 near eddy centers and "eddy pumping" (Martin and Richards, 2001; McGillicuddy et al.,
748 2007, 1998) of nutrients into the photic layer. Its effects are most commonly observed near
749 eddy centers where enhanced chlorophyll can be found. Conversely in downwelling eddies
750 (anticyclonic in the southern hemisphere) poorer waters are expected.Lateral advection of
751 pre-existing primary production gradients by eddies (Chelton et al., 2011a) or advective
752 concentration/dispersion of floating materials (Dandonneau et al., 2003) are also common
753 mechanisms and linked to mesoscale phenomena. Maximum impacts on phytoplankton are
754 expected at the eddy edge or out of eddies in association with the frontal submesoscale
755 dynamics. Vertical pumping may also occur within submesoscale structures produced by
756 eddy-eddy interactions through frontal and ageostrophic mechanisms (*e.g.* Klein and
757 Lapeyre, 2009; Lévy, 2008).

758 A number of eddies and frontal oceanographic processes were observed during the Nectalis
759 cruises. The sampling resolution of both *in situ* and satellite data during the Nectalis cruises
760 was sufficient to observe mesoscale eddies (20-100 km scale). However the sampling
761 resolution was insufficient to differentiate between submesoscale fronts (2-20 km scale,
762 Lévy, 2008) and lateral advection.

763 Enhanced primary production was observed mainly south of ~20°S in the New Caledonia EEZ
764 at the center of several cyclonic eddies (e.g. Nectalis1 eddy A; Nectalis2 eddy D; Nectalis2
765 eddy G) suggesting the occurrence of eddy pumping. Lower primary production was
766 observed in the downwelling (anticyclonic) eddy at station 9 during Nectalis2 (eddy K). In
767 downwelling areas lateral advection from fluid convergence can concentrate floating
768 organisms (Dandonneau et al. 2003) such as the diazotrophic cyanobacterium
769 *Trichodesmium* which can be quite frequent in the region (Dupouy et al., 2011). At station 9
770 (Nectalis 2) a higher proportion of large phytoplankton cells with higher concentration of
771 phycoerythrin suggested the presence of *Trichodesmium*, consistent with lateral advection
772 accumulation.

773 Enhanced primary production and chlorophyll were observed more commonly at the edge
774 of several eddies to the north of ~20°S in the more oligotrophic regions. Enhanced primary
775 productivity may have resulted from chlorophyll advected into the area either from the
776 north via a series of cyclonic eddies (e.g. Nectalis2 series of cyclonic eddies H, I, J; Nectalis1
777 station 10 eddy C) or from the south (Nectalis1 stations 6-7 eddy B). The increased
778 proportion of larger phytoplankton cells at Nectalis1 station 10 (eddy C) is consistent with
779 evolution in composition of eddies with time. The phytoplankton community may have
780 developed in the north and aged along the eddy streamlines as it was advected to the south
781 by eddy currents. However this observation was not consistent for all eddies observed with
782 no specific phytoplankton composition observed at some eddies (e.g. Nectalis1 station 6
783 eddy B).

784 Overall, the primary production patterns around New Caledonia appeared to be more highly
785 dominated by horizontal advection rather than by vertical processes (direct eddy pumping).
786 The patchy and high frequency signal complicated the general understanding of the
787 ecosystem organization, as is often the case in oligotrophic waters. More generally, how
788 mesoscale eddies and the submesoscale structures affect primary production is still under
789 debate (Chelton et al., 2011a; Gruber et al., 2011; Klein and Lapeyre, 2009; Lévy, 2008) and
790 the Nectalis data suggests that there is not one particular mechanism at work during the
791 period of the cruises in this region of the South Pacific.

792 The effect of primary production dynamics at these scales on upper trophic levels are also
793 poorly understood because of the difficulty of accessing datasets spanning a wide range of
794 trophic levels at the scales relevant to eddies and submesoscale structures. Similarly to
795 primary production, the few examples of zooplankton organization around eddies (e.g.
796 Lebourges-Dhaussy et al., 2014; Menkes et al., 2002; Roman et al., 1995) show a variety of
797 organizations. The S-ADCP backscatter (not shown), EK60 Sv and SEAPODYM micronekton
798 data showed strong patchiness, especially in the south, indicating the influence of
799 mesoscale features on the organization of zooplankton and micronekton. Similarly to
800 zooplankton, the relationship between mesoscale features and micronekton distribution is

801 considered to be complex and not yet well understood (Béhagle et al., 2014; Domokos,
802 2009; Potier et al., 2014).

803 *4.3 Seasonality*

804 Observations collected during the Nectalis cruises reflected strong seasonality in
805 hydrodynamics and water column characteristics in response to the seasonal migration of
806 the solar heating and convective system of the SPCZ. The hot season was characterized by
807 warmer and fresher ocean conditions, increased eddy activity, lower NPP and
808 phytoplankton biomass, and higher stratification as modelled by Marchesiello et al. (2010),
809 The cool season was characterized by lower eddy activity, higher NPP and phytoplankton
810 biomass. The NPP latitudinal gradient during the cool season mimicked the SST gradient,
811 indicating a tight coupling between ocean dynamics and phytoplankton growth. There was a
812 stronger decoupling between the surface temperature patterns and primary production
813 during the hot season, as expected in oligotrophic waters (Le Borgne et al., 2011).

814 Primary production almost doubled during the cool season compared to the hot season.
815 Contradictory seasonal signals for zooplankton and micronekton biomass, however were
816 provided by various sampling methods, resulting in an inability to determine seasonality in
817 mid-level organisms. Two hypotheses, possibly acting in combination, may explain the
818 observations. Firstly, enhanced net primary production during the cool season may have
819 been largely due to enhanced recycling, with a small portion of the primary production
820 transmitted to higher trophic levels. Secondly, different turn-over times between
821 phytoplankton and zooplankton/micronekton may have induced a time decoupling and a
822 delay in transmission of primary production to secondary and tertiary levels.

823 It should be noted that, at the time of the cruises in 2011, the South Pacific was considered
824 to be in a weak La Niña state
825 (http://iri.columbia.edu/climate/ENSO/currentinfo/archive/201110/technical.html). In the
826 New Caledonia region, the expected response of the ocean to La Niña is a weakening of the
827 trade winds during the hot season and slightly warmer SST conditions (~+0.5°C in average)

828 with a slightly deeper thermocline (Menkes, 2012). This weak effect of ENSO in the New
829 Caledonian area however, is unlikely to bias the seasonal view from the two cruises.

830 *4.4 Diel migration*

831 Classical diel behavior of organisms migrating towards the surface at night and to deep
832 waters during the day was observed in both zooplankton and micronekton using acoustic
833 methods. Using net sampling however, the day-night difference in zooplankton DW was not
834 observed in the zooplankton WW for the 0-200 m depth during the hot season. This may be
835 explained by the increase of gelatinous organisms (mainly salps and doliolids) at the surface
836 during the hot season (H. Smeti, *pers. com.*) and their representation in WW and DW
837 estimates. Because gelatinous organisms comprise the largest group in WW estimates, their
838 diel behavior will dominate any diel signal for zooplankton. As they rarely migrate vertically,
839 little day-night differences in WW would be expected for zooplankton. The proportion of
840 DW biomass contributed by gelatinous organisms however is much smaller. The
841 predominance of diel vertical behavior in the other taxa groups then results in a diel signal
842 being evident in zooplankton DW.

843 *4.5 Measuring primary production, zooplankton and micronekton*

844 Despite the high variability observed in our primary production *in situ* measurements,
845 particularly during the cool season, and despite their small number (12 measures out of 41
846 stations for both cruises), we estimated they were reasonably representative of the entire
847 cruise. *In situ* measures of primary production during both Nectalis cruises were similar to
848 previous studies in the region (300 – 1000 mgC m^{-2} day^{-1} in September 2004 at 28°S and
849 ~155°E-162°E according to Young et al. (2011). These *in situ* measurements were also in the
850 range of values estimated by satellite for the season, providing some validation and allowing
851 confidence in using the satellite VGPM values for a larger scale assessment of primary
852 production.

853 The biomass estimates of microzooplankton and mesozooplankton (~20-2000 µm) provided
854 by the S-ADCP were significantly correlated to the estimates using acoustics (TAPS) and
855 nets. Estimates derived from the S-ADCP however, are likely to include other organisms and

856 therefore the S-ADCP provides a proxy which is not only reflective of zooplankton biomass
857 (e.g. Burd and Thomson, 2012; Chereskin and Tarling, 2007). The strong correlation
858 between the 153kHz S-ADCP Sv and the EK60 signal, the frequencies of which detect a range
859 of organisms from zooplankton to micronekton and larger, indicate that estimates provided
860 by the S-ADCP also include estimates of micronekton biomass. Although the results did not
861 allow us to define precisely which size-range of organisms was detected by the S-ADCP, and
862 despite the difficulties in calibrating the S-ADCP onboard vessels (Gostiaux and van Haren,
863 2010), our results suggest that this instrument may provide a useful proxy of relative
864 biomass of zooplankton and micronekton confirming its use as a functional tool for this
865 purpose (Brierley et al., 1998; Flagg and Smith, 1989; Heywood et al., 1991; Lee et al., 2008;
866 Radenac et al., 2010). Given that the S-ADCP has been used routinely for more than two
867 decades to sample ocean currents, the data provided by these instruments could potentially
868 be useful for mapping zooplankton/micronekton biomass distributions.

869 Correlations between net and acoustic (TAPS) estimates of zooplankton biomass observed
870 in this study have also previously been observed (e.g. Lebourges-Dhaussy et al., 2014;
871 2009a). Preliminary comparisons between the target micronekton trawls and the EK60
872 acoustic signal however, were not correlated. These data need to be further explored. Low
873 but significant correlations between micronekton net sampling and acoustic EK60 Sv have
874 previously been found for micronekton south of New Caledonia using standardized oblique
875 tows from 600 m to the surface at night (Young et al., 2011). Net sampling at targeted depth
876 and selectivity/catchability/avoidance biases are some of the classic issues that may explain
877 the often low correlation between micronekton net sampling and acoustic estimates (Kloser
878 et al., 2009; Koslow et al., 1997).

879 Zooplankton biomass estimates provided by the TAPS were observed to be more than one
880 order of magnitude higher than the biomass estimates provided by net sampling. These
881 results are at odds with previous comparisons in other regions (e.g. Lebourges-Dhaussy et
882 al., 2014, 2009) and at present we do not have a clear explanation for this discrepancy.
883 Several hypotheses can be proposed which might explain such a disagreement. The TAPS
884 detects organisms in the 50-3000 µm size range, while the nets used during the cruises only

885 collected organisms larger than 200 µm. The smaller sized organisms detected by the TAPS
886 but not collected by the net may lead to smaller biomass estimates from net samples.
887 Exploration of the data suggested that differences in the size ranges sampled by each
888 method cannot explain the large difference in the two estimates. A plausible explanation
889 could be the inadequacy of the parameterization of the model used in the inversion
890 algorithm to calculate biomass from the TAPS signal. This would induce an overestimation of
891 the biovolume by the TAPS if, for example, the density contrast between organisms and the
892 water is underestimated. Further exploration of both the data and sampling of the water
893 column by the TAPS is required. Moreover, vertical net sampling of the water column may
894 be insufficient for representatively sample the oligotrophic waters around New Caledonia as
895 the quantity of zooplankton collected was very low. Additional cruises are needed in which
896 alternative sampling methods such as oblique tows which filter larger quantities of water
897 and collect larger quantities of samples can be trialed and investigated.

898 Biomass estimates of micronekton provided by net sampling and those provided by the
899 SEAPODYM ecosystem model were observed to be in the same range. Because the net
900 sampled at specific depths thereby providing estimates which were not representative of
901 the whole water column, and because of the relative simplicity of the way in which
902 micronekton are estimated in SEAPODYM (Lehodey et al., 2010) this was not necessarily
903 expected. Additionally, micronekton biomass estimates provided by SEAPODYM were
904 significantly correlated to the 38 kHz EK60 acoustic signal. Again this was not expected as
905 the ocean currents used to force SEAPODYM and determine micronekton spatial
906 distribution in the sub-model come from a model reanalysis and not observations. Hence
907 good space/time coherence between observed and modeled mesoscale structures at the
908 time of the observations would not necessarily be expected. Given that the SEAPODYM
909 simulation is simply eddy permitting, these results are encouraging and indicate that the
910 influence of mesoscale features on micronekton biomass is adequately captured by
911 SEAPODYM in this region.

912

4.6 A broader view of the south-west Pacific

The correlations observed between observations and both VGPM satellite-derived primary production and SEAPODYM estimates of micronekton biomass provide some confidence in using these products in describing the ocean dynamics of the broader south-west Pacific Ocean (~15°S-35°S and 150°E-175°E) encompassing the Coral Sea.

Looking more broadly than the region in which the cruises were conducted, horizontal advections also shaped the horizontal structure of primary production in the. (Figure 9). Using VGPM satellite-derived primary production data and SEAPODYM micronekton estimates, higher primary production and micronekton values were observed south of 23°S during the cool season and south of 31°S during the hot season than areas further north. Across the overall south west Pacific Ocean region, primary production was much stronger (by approximately a factor 2 to 3) during the cool season compared to the hot season as the SPCZ regime weakened and stronger winds promoted replenishment of surface nutrients (Figure 9). A similar seasonal signal was observed in micronekton biomass as derived from SEAPODYM however, the contrast between seasons was smaller than that observed in primary production estimates (micronekton was higher during the cool season by a factor <2).

Micronekton biomass south of 20°S as provided by SEAPODYM was globally organized in very patchy structures and the primary production maxima provided via remote sensing did not necessarily match the micronekton maxima. One good example can be found in the "downwelling"anticylonic eddy in the EAC at 32°S-155°E, where primary production was organized in a strong band around the eddy whereas micronekton biomass was organized along a filament at the edge of the eddy. Estimates of micronekton biomass provided by SEAPODYM indicated that the southern region was richer in biomass, but was also much more variable than the northern region (Figure 9).

Presence of patchy structures and decoupling between different trophic levels raises uncertainty associated with using snapshot surveys to understand the coherence of an

ecosystem in turbulent regions. Additional observations in the region will be needed to confirm the nature of the ecosystem organization at (sub) mesoscales.

5 Conclusions and perspectives

By collecting new data extending from the ocean dynamics to micronekton in the top 600 m, the two Nectalis cruises conducted in the south-west Pacific Ocean in austral cool and hot season of 2011 have provided a better understanding of the pelagic offshore ecosystem of this oligotrophic region. Multiple methods were used to measure zooplankton and micronekton (S-ADCP, TAPS, zooplankton net, SIMRAD EK60, micronekton net). Correlations were found between methods, however, net biomass estimates and acoustic-derived estimates did not compare very well. On the other hand, estimates of micronekton provided from net sampling and SEAPODYM were in the same range. The S-ADCP reproduced adequately the trends observed in micronekton and zooplankton, but was unable to distinguish zooplankton from micronekton and absolute biomasses could therefore not be calculated. Calibration of the different methods used to estimate zooplankton and micronekton will require additional and more specifically designed studies. Based on large existing S-ADCP datasets, the demonstrated relation between the S-ADCP signal and the zooplankton/micronekton biomass estimates provides the opportunity to estimate relative zooplankton/micronekton biomasses on much larger scales than those available from dedicated instruments such as EK60 or TAPS. Such effort will be undertaken in the New Caledonia region using the available S-ADCP database spanning the past 20 years. In line with this work, we believe that the development of on-board calibration methods for the S-ADCP similar to those for echosounders (e.g. EK60) would be of great interest, particularly in providing absolute measures of abundance. Models such as SEAPODYM would benefit from absolute biomasses to better calibrate energy transfer parameterizations.

Based on our limited dataset and the resolution of our data, we could not examine the systematic effects of submesoscale phenomenon such as eddies and fronts on ocean

968 biochemistry and planktonic/nektonic communities structures during the Nectalis cruises.
969 Data collected however, did suggest that horizontal advection was dominant over eddy
970 pumping. Our study highlights the difficulty of understanding the impact of eddies in
971 oligotrophic conditions without a full three dimensional dataset. We were also unable to
972 explore the role that spatial variability might have at the submesoscale (frontal) level, a
973 scale at which ecosystems have been shown to organize in some cases (e.g. Lebourges-
974 Dhaussy et al., 2014; Lévy et al., 2012; Tew Kai et al., 2009). This remains an open question
975 of wide scientific interest. Further, two cruises in two seasons are not sufficient to fully
976 describe the role of seasonality on the ecosystem. Additional *in situ* measurements will be
977 required to further understand the magnitude of the spatial distribution and seasonal cycle
978 of zooplankton/micronekton biomass in the region, as planned in the coming years within
979 the framework of the Nectalis program.

980 The synoptic Nectalis cruises and the SEAPODYM model at the regional scale indicated that
981 the micronekton structure south of 20°S was remarkably patchy during both seasons in
982 relation to the mesoscale dynamics of the region. This patchiness raises the question of how
983 to best sample the region with dedicated cruises. At present, we have chosen to broadly
984 sample the New Caledonian EEZ. We believe that given the large uncertainty in
985 understanding of the ecosystem organization and species, it is still useful to pursue this
986 effort and will be carried out in a series of two additional cruises in the coming years. We
987 also do note that is it extremely difficult to interpret ecosystem signals at the mesoscale
988 level using transects organized to cover wide spatial areas. We therefore aim to design
989 dedicated cruises to follow a number of eddies in the region and understand the time
990 dynamics of such evolving systems.

991

992 **Acknowledgements**

993 This research was co-funded by the Institute of Research for Development (IRD), the LEFE-
994 CYBER program, the Agence des Aires Marines Protégées (AAMP) and the New Caledonian
995 Zone Economique de Nouvelle-Caledonie (ZoNeCo) program. H. Smeti received support

from IRD through its PhD. scholarship program. B. Hunt was supported by a Marie Curie Fellowship (ISOZOO) of the 7th International Framework Programme. V. Allain was supported by the Australian Overseas Aid Program (AUSAID). We thank Magali Teurlai (IRD, UMR LOCEAN/UMR ESPACE-DEV) for guidance on statistical analyses, Aude Barani (PRECYM) for analyses as well as Philippe Gérard (IRD, US LAMA). We are grateful to the captain, Jean-François Barazer (IRD), and the crew of the R/V Alis for their work during the cruises, to Yves Gouriou (IRD) for the preparation of the cruises, to Elodie Vourey (SPC) and Jeff Dubosc (SPC) for their assistance with identification of micronekton organisms. We also thank the two anonymous reviewers and Karen Evans (CSIRO) whose comments significantly improved this manuscript.

References

Abecassis, M., Senina, I., Lehodey, P., Gaspar, P., Parker, D., Balazs, G., Polovina, J., 2013. A model of loggerhead sea turtle (*Caretta caretta*) habitat and movement in the oceanic North Pacific. PLoS ONE 8, e73274. doi:10.1371/journal.pone.0073274

Allain, V., Fernandez, E., Hoyle, S.D., Caillot, S., Jurado-Molina, J., Andréfouët, S., Nicol, S.J., 2012. Interaction between coastal and oceanic ecosystems of the Western and Central Pacific Ocean through predator-prey relationship studies. PLos ONE 7, e36701.

Aminot, A., Kérouel, R., 2007. Dosage automatique des nutriments dans les eaux marines: méthodes en flux continu. IFREMER, Paris.

Barnier, B., Madec, G., Penduff, T., Molines, J.-M., Treguier, A.-M., Sommer, J.L., Beckmann, A., Biastoch, A., Böning, C., Dengg, J., Derval, C., Durand, E., Gulev, S., Remy, E., Talandier, C., Theetten, S., Maltrud, M., McClean, J., Cuevas, B.D., 2006. Impact of partial steps and momentum advection schemes in a global ocean circulation model at eddy-permitting resolution. Ocean Dyn. 56, 543–567. doi:10.1007/s10236-006-0082-1

Béhagle, N., du Buisson, L., Josse, E., Lebourges-Dhaussy, A., Roudaut, G., Ménard, F., 2014. Mesoscale features and micronekton in the Mozambique Channel: An acoustic approach. Deep Sea Res. Part II 100, 164–173. doi:10.1016/j.dsr2.2013.10.024

Behrenfeld, M., Falkowski, P.G., 1997. A consumer's guide to phytoplankton primary productivity models. Limnol. Oceanogr. 42, 1479–1491. doi:10.4319/lo.1997.42.7.1479

Bell, J.D., Reid, C., Batty, M.J., Lehodey, P., Rodwell, L., Hobday, A.J., Johnson, J.E., Demmke, A., 2013. Effects of climate change on oceanic fisheries in the tropical Pacific: implications for economic development and food security. Clim. Change 119, 199–212. doi:10.1007/s10584-012-0606-2

Bertrand, A., Le Borgne, R., Josse, E., 1999. Acoustic characterisation of micronekton distribution in French Polynesia. Mar. Ecol. Prog. Ser. 191, 127–140.

Briand, K., Molony, B., Lehodey, P., 2011. A study on the variability of albacore (*Thunnus alalunga*) longline catch rates in the southwest Pacific Ocean. Fish. Oceanogr. 20, 517–529. doi:10.1111/j.1365-2419.2011.00599.x

Brierley, A.S., Brandon, M.A., Watkins, J.L., 1998. An assessment of the utility of an acoustic Doppler current profiler for biomass estimation. Deep Sea Res. Part I 45, 1555–1573. doi:10.1016/S0967-0637(98)00012-0

Burd, B., Thomson, R., 2012. Estimating zooplankton biomass distribution in the water column near the endeavour segment of Juan de Fuca Ridge using acoustic backscatter and concurrently towed nets. Oceanography 25, 269–276. doi:10.5670/oceanog.2012.25

Campbell, L., Carpenter, E.J., Montoya, J.P., Kustka, A.B., Capone, D.G., 2005. Picoplankton community structure within and outside a *Trichodesmium* bloom in the southwestern Pacific Ocean. Life Environ. 55, 185–195.

Carassou, L., Le Borgne, R., Rolland, E., Ponton, D., 2010. Spatial and temporal distribution of zooplankton related to the environmental conditions in the coral reef lagoon of

New Caledonia, Southwest Pacific. Mar. Pollut. Bull. 61, 367–374. doi:10.1016/j.marpolbul.2010.06.016

Ceccarelli, D.M., McKinnon, A.D., Andréfouët, S., Allain, V., Young, J., Gledhill, D.C., Flynn, A., Bax, N.J., Beaman, R., Borsa, P., Brinkman, R., Bustamante, R.H., Campbell, R., Cappo, M., Cravatte, S., D'Agata, S., Dichmont, C.M., Dunstan, P.K., Dupouy, C., Edgar, G., Farman, R., Furnas, M., Garrigue, C., Hutton, T., Kulbicki, M., Letourneur, Y., Lindsay, D., Menkes, C., Mouillot, D., Parravicini, V., Payri, C., Pelletier, B., Richer de Forges, B., Ridgway, K., Rodier, M., Samadi, S., Schoeman, D., Skewes, T., Swearer, S., Vigliola, L., Wantiez, L., Williams, A., Williams, A., Richardson, A.J., 2013. The Coral Sea: physical environment, ecosystem status and biodiversity assets, in: Michael Lesser (Ed.), Advances in Marine Biology. Academic Press, pp. 213–290.

Chelton, D.B., Gaube, P., Schlax, M.G., Early, J.J., Samelson, R.M., 2011a. The influence of nonlinear mesoscale eddies on near-surface oceanic chlorophyll. Science 334, 328–332. doi:10.1126/science.1208897

Chelton, D.B., Schlax, M.G., Samelson, R.M., 2011b. Global observations of nonlinear mesoscale eddies. Prog. Oceanogr. 91, 167–216. doi:10.1016/j.pocean.2011.01.002

Chereskin, T.K., Tarling, G.A., 2007. Interannual to diurnal variability in the near-surface scattering layer in Drake Passage. ICES J Mar Sci 64, 1617–1626.

Couvelard, X., Marchesiello, P., Gourdeau, L., Lefèvre, J., 2008. Barotropic zonal jets induced by islands in the Southwest Pacific. J. Phys. Oceanogr. 38, 2185–2204. doi:10.1175/2008JPO3903.1

D' Ovidio, F., De Monte, S., Penna, A.D., Cotté, C., Guinet, C., 2013. Ecological implications of eddy retention in the open ocean: a Lagrangian approach. J. Phys. Math. Theor. 46, 254023. doi:10.1088/1751-8113/46/25/254023

Dandonneau, Y., Gohin, F., 1984. Meridional and seasonal variations of the sea surface chlorophyll concentration in the southwestern tropical Pacific (14 to 32°S, 160 to 175°E). Deep Sea Res. Part A 31, 1377–1393. doi:10.1016/0198-0149(84)90078-5

Dandonneau, Y., Vega, A., Loisel, H., Penhoat, Y. du, Menkes, C., 2003. Oceanic Rossby waves acting as a "hay rake" for ecosystem floating by-products. Science 302, 1548–1551. doi:10.1126/science.1090729

De Boyer Montégut, C., Madec, G., Fischer, A.S., Lazar, A., Iudicone, D., 2004. Mixed layer depth over the global ocean: An examination of profile data and a profile-based climatology. J. Geophys. Res. Oceans 109, C12003. doi:10.1029/2004JC002378

Deines, K.L., 1999. Backscatter estimation using Broadband acoustic Doppler current profilers, in: Anderson, S.P., Terray, E.A., Rizoli White, J.A., Williams 3rd, A.J. (Eds.), Proceedings of the IEEE Sixth Working Conference on Current Measurement, 1999. IEEE, Piscataway, pp. 249–253. doi:10.1109/CCM.1999.755249

Domokos, R., 2009. Environmental effects on forage and longline fishery performance for albacore (*Thunnus alalunga*) in the American Samoa Exclusive Economic Zone. Fish. Oceanogr. 18, 419–438.

Dupouy, C., Benielli-Gary, D., Neveux, J., Dandonneau, Y., Westberry, T.K., 2011. An algorithm for detecting Trichodesmium surface blooms in the South Western Tropical Pacific. Biogeosciences 8, 3631–3647. doi:10.5194/bg-8-3631-2011

1094 Dutrieux, P., Menkes, C.E., Vialard, J., Flament, P., Blanke, B., 2008. Lagrangian study of
1095 tropical instability vortices in the Atlantic. J. Phys. Oceanogr. 38, 400–417.
1096 doi:10.1175/2007JPO3763.1
1097 Farley, J.H., Williams, A.J., Hoyle, S.D., Davies, C.R., Nicol, S.J., 2013. Reproductive dynamics
1098 and potential annual fecundity of South Pacific albacore tuna (*Thunnus alalunga*).
1099 PLoS ONE 8, e60577. doi:10.1371/journal.pone.0060577
1100 Ferry, N., Parent, L., Garric, M., Drevillon, C., Desportes, C., Bricaud, F., Hernandez, F., 2012.
1101 Scientific Validation Report (ScVR) for reprocessed analysis and reanalysis. MyOcean
1102 Proj. Rep. MYO-WP04-ScCV-Rea-Mercat.-V10 1–66.
1103 Flagg, C.N., Smith, S.L., 1989. On the use of the acoustic doppler current profiler to measure
1104 zooplankton abundance. Deep Sea Res. Part A 36, 455–474. doi:10.1016/0198-
1105 0149(89)90047-2
1106 Flynn, A.J., Paxton, J.R., 2012. Spawning aggregation of the lanternfish *Diaphus danae*
1107 (family Myctophidae) in the north-western Coral Sea and associations with tuna
1108 aggregations. Mar. Freshw. Res. 63, 1255–1271.
1109 Foote, K.G., Knudsen, H.P., Vestnes, D.N., MacLennan, D.N., Simmonds, E.J., 1987.
1110 Calibration of acoustic instruments for fish density estimation: a practical guide. ICES
1111 Coop. Res. Rep. 144.
1112 Ganachaud, A., Vega, A., Rodier, M., Dupouy, C., Maes, C., Marchesiello, P., Eldin, G.,
1113 Ridgway, K., Le Borgne, R., 2010. Observed impact of upwelling events on water
1114 properties and biological activity off the southwest coast of New Caledonia. Mar.
1115 Pollut. Bull. 61, 449–464. doi:10.1016/j.marpolbul.2010.06.042
1116 Gillett, R., 2009. Fisheries in the economies of the Pacific island countries and territories.
1117 Asian Development Bank, Mandaluyong City.
1118 Gostiaux, L., van Haren, H., 2010. Extracting meaningful information from uncalibrated
1119 backscattered echo intensity data. J. Atmospheric Ocean. Technol. 27, 943–949.
1120 doi:10.1175/2009JTECHO704.1
1121 Gourdeau, L., Kessler, W.S., Davis, R.E., Sherman, J., Maes, C., Kestenare, E., 2008. Zonal jets
1122 entering the Coral Sea. J. Phys. Oceanogr. 38, 715–725. doi:10.1175/2007JPO3780.1
1123 Grandperrin, R., 1969. Couches diffusantes dans le Pacifique équatorial et sud-tropical. Cah.
1124 ORSTOM Sér. Océan. VII, 99–112.
1125 Grandperrin, R., 1975. Structures trophiques aboutissant aux thons de longue ligne dans le
1126 Pacifique sud-ouest tropical. Thèse Détat Univ. Aix-Marseille II 1–296.
1127 Gruber, N., Lachkar, Z., Frenzel, H., Marchesiello, P., Münnich, M., McWilliams, J.C., Nagai,
1128 T., Plattner, G.-K., 2011. Eddy-induced reduction of biological production in eastern
1129 boundary upwelling systems. Nat. Geosci. 4, 787–792. doi:10.1038/ngeo1273
1130 Heywood, K.J., Scrope-Howe, S., Barton, E.D., 1991. Estimation of zooplankton abundance
1131 from shipborne ADCP backscatter. Deep Sea Res. Part A 38, 677–691.
1132 doi:10.1016/0198-0149(91)90006-2
1133 Holliday, D.V., Pieper, R.E., 1980. Volume scattering strengths and zooplankton distributions
1134 at acoustic frequencies between 0.5 and 3 MHz. J. Acoust. Soc. Am. 135–146.
1135 Holliday, D.V., Pieper, R.E., Kleppel, G.S., 1989. Determination of zooplankton size and
1136 distribution with multifrequency acoustic technology. ICES J. Mar. Sci. 46, 52–61.
1137 doi:10.1093/icesjms/46.1.52

Hummon, J.M., Firing, E., 2003. A direct comparison of two RDI shipboard ADCPs: a 75-kHz ocean surveyor and a 150-kHz narrow band. J. Atmospheric Ocean. Technol. 20, 872–888.

Hunt, B.P.V., Allain, V., Lorrain, A., Menkes, C., Rodier, M., Pagano, M., Carlotti, F., Graham, B.S., this issue. Size-structured interactions in a sub-tropical pelagic food web. Deep Sea Res. Part II.

Hydro-Bios Apparatebau GmbH, 2009. Multi plankton sampler Multinet Type Midi. Operation manual. Hydro-Bios Apparatebau GmbH, Kiel-Altenholz.

Jacquet, S., Delesalle, B., Torrton, J., Blanchot, J., 2006. Response of phytoplankton communities to increased anthropogenic influences (southwestern lagoon, New Caledonia). Mar. Ecol. Prog. Ser. 320, 65–78. doi:10.3354/meps320065

Kessler, W.S., Cravatte, S., 2013. Mean circulation of the Coral Sea. J. Geophys. Res. Oceans 118, 6385–6410. doi:10.1002/2013JC009117

Killworth, P.D., Cipollini, P., Uz, B.M., Blundell, J.R., 2004. Physical and biological mechanisms for planetary waves observed in satellite-derived chlorophyll. J. Geophys. Res. Oceans 109, C07002. doi:10.1029/2003JC001768

Klein, P., Lapeyre, G., 2009. The oceanic vertical pump induced by mesoscale and submesoscale turbulence. Annu. Rev. Mar. Sci. 1, 351–375. doi:10.1146/annurev.marine.010908.163704

Kloser, R., Ryan, T., Young, J.W., Lewis, M.E., 2009. Acoustic observations of micronekton fish on the scale of an ocean basin: potential and challenges. ICES J. Mar. Sci. 66, 998–1006.

Koslow, J.A., Kloser, R.J., Williams, A., 1997. Pelagic biomass and community structure over the mid-continental slope off southeastern Australia based upon acoustic and midwater trawl sampling. Mar. Ecol.-Prog. Ser. 146, 21–35. doi:10.3354/meps146021

Le Borgne, R., Allain, V., Matear, R.J., Griffiths, S.P., McKinnon, A.D., Richardson, A.J., Young, J.W., 2011. Vulnerability of open ocean food webs in the tropical Pacific to climate change, in: Bell, J., Johnson, J.E., Hobday, A.J. (Eds.), Vulnerability of Fisheries and Aquaculture in the Tropical Pacific to Climate Change. Secretariat of the Pacific Community, Noumea, pp. 189–250.

Le Bouteiller, A., Blanchot, J., Rodier, M., 1992. Size distribution patterns of phytoplankton in the western Pacific: towards a generalization for the tropical open ocean. Deep Sea Res. Part A 39, 805–823. doi:10.1016/0198-0149(92)90123-B

Lebourges-Dhaussy, A., Coetzee, J., Hutchings, L., Roudaut, G., Nieuwenhuys, C., 2009. Zooplankton spatial distribution along the South African coast studied by multifrequency acoustics, and its relationships with environmental parameters and anchovy distribution. ICES J. Mar. Sci. 66, 1055–1062. doi:10.1093/icesjms/fsp129

Lebourges-Dhaussy, A., Huggett, J., Ockhuis, S., Roudaut, G., Josse, E., Verheye, H., 2014. Zooplankton size and distribution within mesoscale structures in the Mozambique Channel: A comparative approach using the TAPS acoustic profiler, a multiple net sampler and ZooScan image analysis. Deep Sea Res. Part II 100, 136–152. doi:10.1016/j.dsr2.2013.10.022

1181 Lee, K., Mukai, T., Lee, D., Iida, K., 2008. Verification of mean volume backscattering
1182 strength obtained from acoustic doppler current profiler by using sound scattering
1183 layer. Fish. Sci. 74, 221–229. doi:10.1111/j.1444-2906.2008.01516.x
1184 Legand, M., Bourret, P., Grandperrin, R., Rivaton, J., 1970. A preliminary study of some
1185 micronektonic fishes in the equatorial and tropical western Pacific, in: Scientific
1186 Exploration of the South Pacific. National Academy of sciences, Washington,D.C., pp.
1187 225–235.
1188 Lehodey, P., Andre, J.-M., Bertignac, M., Hampton, J., Stoens, A., Menkes, C., Memery, L.,
1189 Grima, N., 1998. Predicting skipjack tuna forage distributions in the equatorial Pacific
1190 using a coupled dynamical bio-geochemical model. Fish. Oceanogr. 7, 317–325.
1191 doi:10.1046/j.1365-2419.1998.00063.x
1192 Lehodey, P., Murtugudde, R., Senina, I., 2010. Bridging the gap from ocean models to
1193 population dynamics of large marine predators: a model of mid-trophic functional
1194 groups. Prog. Oceanogr. 84, 69–84.
1195 Lehodey, P., Senina, I., Murtugudde, R., 2008. A spatial ecosystem and populations
1196 dynamics model (SEAPODYM) – Modeling of tuna and tuna-like populations. Prog.
1197 Oceanogr. 78, 304–318. doi:10.1016/j.pocean.2008.06.004
1198 Lévy, M., 2008. The modulation of biological production by oceanic mesoscale turbulence,
1199 in: Weiss, J.B., Provenzale, A. (Eds.), Transport and Mixing in Geophysical Flows.
1200 Springer Berlin Heidelberg, pp. 219–261.
1201 Lévy, M., Ferrari, R., Franks, P.J.S., Martin, A.P., Rivière, P., 2012. Bringing physics to life at
1202 the submesoscale. Geophys. Res. Lett. 39, L14602. doi:10.1029/2012GL052756
1203 MacLennan, D.N., Fernandes, P.G., Dalen, J., 2002. A consistent approach to definitions and
1204 symbols in fisheries acoustics. ICES J. Mar. Sci. 59, 365–369.
1205 doi:10.1006/jmsc.2001.1158
1206 Marchesiello, P., Lefèvre, J., Vega, A., Couvelard, X., Menkes, C., 2010. Coastal upwelling,
1207 circulation and heat balance around New Caledonia's barrier reef. Mar. Pollut. Bull.
1208 61, 432–448. doi:10.1016/j.marpolbul.2010.06.043
1209 Martin, A.P., Richards, K.J., 2001. Mechanisms for vertical nutrient transport within a North
1210 Atlantic mesoscale eddy. Deep Sea Res. Part II 48, 757–773. doi:10.1016/S0967-
1211 0645(00)00096-5
1212 McClatchie, S., Dunford, A., 2003. Estimated biomass of vertically migrating mesopelagic fish
1213 off New Zealand. Deep Sea Res. Part I 50, 1263–1281. doi:10.1016/S0967-
1214 0637(03)00128-6
1215 McGillicuddy, D.J., Anderson, L.A., Bates, N.R., Bibby, T., Buesseler, K.O., Carlson, C.A., Davis,
1216 C.S., Ewart, C., Falkowski, P.G., Goldthwait, S.A., Hansell, D.A., Jenkins, W.J., Johnson,
1217 R., Kosnyrev, V.K., Ledwell, J.R., Li, Q.P., Siegel, D.A., Steinberg, D.K., 2007.
1218 Eddy/wind interactions stimulate extraordinary mid-ocean plankton blooms. Science
1219 316, 1021–1026. doi:10.1126/science.1136256
1220 McGillicuddy, D.J., Robinson, A.R., Siegel, D.A., Jannasch, H.W., Johnson, R., Dickey, T.D.,
1221 McNeil, J., Michaels, A.F., Knap, A.H., 1998. Influence of mesoscale eddies on new
1222 production in the Sargasso Sea. Nature 394, 263–266. doi:10.1038/28367
1223 McKinnon, A.D., 2005. Mesozooplankton dynamics in nearshore waters of the Great Barrier
1224 Reef. Estuar. Coast. Shelf Sci. 497–511. doi:10.1016/j.ecss.2004.12.011

McPherson, G.R., 1991. A possible mechanism for the aggregation of yellowfin and bigeye tuna in the north-western Coral Sea. Queensland Department of Primary Industries - Information Series. QI91013, 1–11.

Menkes, C., 2012. Les grandes fluctuations des hydroclimats : le phénomène ENSO, in: Bonvallot, J., Gay, J.-C., Habert, E. (Eds.), Atlas de la Nouvelle Calédonie. IRD, Marseille, pp. 49–52.

Menkes, C.E., Kennan, S.C., Flament, P., Dandonneau, Y., Masson, S., Biessy, B., Marchal, E., Eldin, G., Grelet, J., Montel, Y., Morlière, A., Lebourges-Dhaussy, A., Moulin, C., Champalbert, G., Herbland, A., 2002. A whirling ecosystem in the equatorial Atlantic. Geophys.Res.Lett. 29, 1553.

Moutin, T., Broeck, N.V.D., Beker, B., Dupouy, C., Rimmelin, P., Bouteiller, A.L., 2005. Phosphate availability controls *Trichodesmium spp.* biomass in the SW Pacific Ocean. Mar. Ecol. Prog. Ser. 297, 15–21. doi:10.3354/meps297015

Murphy, J., Riley, J.P., 1962. A modified single solution method for the determination of phosphate in natural waters. Anal. Chim. Acta 27, 31–36. doi:10.1016/S0003-2670(00)88444-5

Napp, J.M., Ortner, P.B., Pieper, R.E., Holliday, D.V., 1993. Biovolume-size spectra of epipelagic zooplankton using a multi-frequency acoustic profiling system (MAPS). Deep Sea Res. Part I 40, 445–459. doi:10.1016/0967-0637(93)90141-O

Neveux, J., Tenorio, M.M.B., Jacquet, S., Torreton, J.-P., Douillet, P., Ouillon, S., Dupouy, C., 2009. Chlorophylls and phycoerythrins as markers of environmental forcings including cyclone Erica effect (March 2003) on phytoplankton in the Southwest lagoon of New Caledonia and oceanic adjacent area. Int. J. Oceanogr. 2009 (Article ID 232513), 19p. doi:10.1155/2009/232513

Olson, R.J., Duffy, L.M., Kuhnert, P.M., Galván-Magaña, F., Bocanegra-Castillo, N., Alatorre-Ramírez, V., 2014. Decadal diet shift in yellowfin tuna (*Thunnus albacares*) suggests broad-scale food web changes in the eastern tropical Pacific Ocean. Mar. Ecol. Prog. Ser. 497, 157–178.

Pieper, R.E., Holliday, D.V., Kleppel, G.S., 1990. Quantitative zooplankton distributions from multifrequency acoustics. J. Plankton Res. 12, 433–441. doi:10.1093/plankt/12.2.433

Pieper, R.E., McGehee, D.E., Greenlaw, C.F., Holliday, D.V., 2001. Acoustically measured seasonal patterns of Zooplankton in the Arabian Sea. Deep Sea Res. Part II 48, 1325–1343. doi:10.1016/S0967-0645(00)00141-7

Potier, M., Bach, P., Ménard, F., Marsac, F., 2014. Influence of mesoscale features on micronekton and large pelagic fish communities in the Mozambique Channel. Deep Sea Res. Part II 100, 184–199. doi:10.1016/j.dsr2.2013.10.026

Qiu, B., Chen, S., Kessler, W.S., 2009. Source of the 70-Day mesoscale eddy variability in the Coral Sea and the north Fiji Basin. J. Phys. Oceanogr. 39, 404–420. doi:10.1175/2008JPO3988.1

Qu, T., Lindstrom, E.J., 2002. A climatological interpretation of the circulation in the western South Pacific. J. Phys. Oceanogr. 32, p2492.

Radenac, M.-H., Plimpton, P.E., Lebourges-Dhaussy, A., Commien, L., McPhaden, M.J., 2010. Impact of environmental forcing on the acoustic backscattering strength in the equatorial Pacific: Diurnal, lunar, intraseasonal, and interannual variability. Deep Sea Res. Part I 57, 1314–1328.

1270 Raimbault, P., Slawyk, G., Coste, B., Fry, J., 1990. Feasibility of using an automated
1271 colorimetric procedure for the determination of seawater nitrate in the 0 to 100 nM
1272 range: examples from field and culture. Mar. Biol. 104, 347–351.
1273 doi:10.1007/BF01313277
1274 Ridgway, K., Dunn, J.R., 2003. Mesoscale structure of the mean East Australian Current
1275 System and its relationship with topography. Prog. Oceanogr. 189–222.
1276 doi:10.1016/S0079-6611(03)00004-1
1277 Ridgway, K.R., Dunn, J.R., Wilkin, J.L., 2002. Ocean interpolation by four-dimensional
1278 weighted least squares—application to the waters around Australasia. J.
1279 Atmospheric Ocean. Technol. 19, 1357–1375.
1280 RochelleNewall, E.J., Torrton, J.P., Mari, X., Pringault, O., 2008. Phytoplankton-
1281 bacterioplankton coupling in a subtropical South Pacific coral reef lagoon. Aquat.
1282 Microb. Ecol. 50, 221–229. doi:10.3354/ame01158
1283 Roger, C., 1974. Répartitions bathymétriques et migrations verticales des Euphausiacés
1284 (crustacés) dans les zones de pêche au thon du Pacifique sud-tropical. Cah. ORSTOM
1285 Sér. Océan. XII, 221–239.
1286 Roger, C., 1986. Macroplancton et micronecton dans le Pacifique Tropical Sud-Ouest.
1287 Oceanogr. Trop. 21, 153–165.
1288 Roman, M.R., Dam, H.G., Gauzens, A.L., Urban-Rich, J., Foley, D.G., Dickey, T.D., 1995.
1289 Zooplankton variability on the equator at 140°W during the JGOFS EqPac study.
1290 Deep Sea Res. Part II 42, 673–693. doi:10.1016/0967-0645(95)00025-L
1291 Rouyer, T., Fromentin, J.-M., Ménard, F., Cazelles, B., Briand, K., Pianet, R., Planque, B.,
1292 Stenseth, N.C., 2008. Complex interplays among population dynamics,
1293 environmental forcing, and exploitation in fisheries. Proc. Natl. Acad. Sci. 105, 5420–
1294 5425. doi:10.1073/pnas.0709034105
1295 Senina, I., Sibert, J., Lehodey, P., 2008. Parameter estimation for basin-scale ecosystem-
1296 linked population models of large pelagic predators: application to skipjack tuna.
1297 Prog. Oceanogr. 78, 319–335.
1298 Simmonds, E.J., MacLennan, D., 2005. Fisheries acoustics theory and practice. Blackwell,
1299 Oxford.
1300 Sutor, M.M., Cowles, T.J., Peterson, W.T., Pierce, S.D., 2005. Acoustic observations of
1301 finescale zooplankton distributions in the Oregon upwelling region. Deep Sea Res.
1302 Part II 52, 109–121. doi:10.1016/j.dsr2.2004.09.029
1303 Tew Kai, E., Rossi, V., Sudre, J., Weimerskirch, H., Lopez, C., Hernandez-Garcia, E., Marsac, F.,
1304 Garçon, V., 2009. Top marine predators track Lagrangian coherent structures. Proc.
1305 Natl. Acad. Sci. 106, 8245–8250. doi:10.1073/pnas.0811034106
1306 Wyman, M., 1992. An in vivo method for the estimation of phycoerythrin concentrations in
1307 marine cyanobacteria (*Synechococcus spp.*). Limnol. Oceanogr. 37, 1300–1306.
1308 Young, J.W., Hobday, A.J., Campbell, R.A., Kloser, R.J., Bonham, P.I., Clementson, L.A.,
1309 Lansdell, M.J., 2011. The biological oceanography of the East Australian Current and
1310 surrounding waters in relation to tuna and billfish catches off eastern Australia. Deep
1311 Sea Res. Part II 58, 720–733.
1312 Young, J.W., Hunt, B.P.V., Cook, T., Llopiz, J., Hazen, E.L., Pethybridge, H., Ceccarelli, D.,
1313 Lorrain, A., Olson, R.J., Allain, V., Menkes, C., Patterson, T., Nicol, S., Lehodey, P.,

Kloser, R., Arrizabalaga, H., Choy, C.A., this issue. The trophodynamics of marine top predators: advances and challenges. Deep-Sea Res. Part II.

Young, J.W., Lansdell, M., Campbell, R., Cooper, S., Juanes, F., Guest, M., 2010. Feeding ecology and niche segregation in oceanic top predators off eastern Australia. Mar. Biol. 157, 2347–2368.

1321 Table 1. Summary of the cruise activities.

	Nectalis1	Nectalis2
Number of sampling stations	18	23
Physics:		
Temperature, salinity, fluorescence, oxygen 0-500 m: CTD sensors	All stations	All stations
Currents: 153 kHz ship borne-ADCP (16-200 m)	Along the track	Along the track
Sea surface salinity and temperature: thermosalinograph	Along the track	Along the track
Nutrients:		
Nutrients, NOx, SRP, 8 depths: 180 m, 150 m, 130 m, 90 m, 70 m, 40 m, 3 m; CTD water sampling	All stations	All stations
Phytoplankton & pigments:		
Total Chlorophyll, 8 depths, fluorometry	All stations	All stations
Size fractionated chlorophyll (<3 µm, 3-10 µm, >10 µm): 8 depths, fluorometry	Stations 2, 4, 6, 8, 10, 12, 14, 16	Stations 1, 2, 6, 9, 11, 14, 17, 20, 23
Pigments: Phycoerythrin, 4 depths in the euphotic zone depending of the stratification (3m, between 20-40m, DCM, below DCM) spectrofluorometry.	Every other station	Every other station
Cell counts: CTD water sampling and flow cytometry	Stations 1, 3, 5, 7, 9 11, 13, 14, 15, 17, 18	Stations 1, 3, 5, 7, 9, 11, 15, 17, 19, 21, 23
Primary production:		
3 depths (surface, between 20-40m, DCM), ^{14}C tracer technique	Stations 1, 4, 7, 9, 13, 16, 17	Stations 4,8,12,15, 21
Zooplankton:		
Net sampling: Hydrobios 5 layer (0-600 m) mesh > 200 µm	All stations	All stations
Acoustics: 1 frequency 153 kHz S-ADCP (16-200 m)	Along the track	Along the track
Acoustics: 6 frequency zooplankton profiler TAPS (0-200 m)	All stations	All stations
Micronekton:		
Net sampling: micronekton net between 14 and 540 m depth (10 mm codend mesh size)	All stations	All stations
Acoustics: 4 frequency EK60 SIMRAD echosounder (0-600 m)	Along the track	Along the track
Acoustics: 1 frequency 153 kHz S-ADCP (16-200 m)	Along the track	Along the track

1322

1323

1324 Table 2. Mean and standard deviation (SD) of primary production, biomass estimates and
1325 acoustic signal of zooplankton and micronekton during the cool season (Nectalis1) and the
1326 hot season (Nectalis2). Results of the Mann-Whitney statistical test (for α=5%) comparing
1327 Nectalis 1 (N1) and Nectalis2 (N2) and percentage of the number of tests producing this
1328 result for datasets with spatial auto-correlation (see section 2.3.1 for detailed explanation).
1329 Seasonal difference between micronekton biomass estimates derived from net sampling
1330 was not undertaken because different times and depths were sampled during each survey.
1331 DW: dry weight; WW: wet weight.

	Nectalis1		Nectalis2		Seasonal difference (Mann-Whitney) and percentage of tests producing the result
	Mean	SD	Mean	SD	
In situ primary production (mgC m^{-2} d^{-1})	352	160	231	133	N1>N2
Satellite derived primary production along the cruise track (mgC m^{-2} d^{-1})	301	62	199	55	100% N1>N2
Sv ADCP (dB)	-82.2	3.5	-83.4	2.8	80% N1>N2; 20% No difference
TAPS biovolume (mg m^{-3})	107.7	37.3	106.7	22.6	No difference
Zooplankton DW. 0-200 m (mg m^{-3})	3.9	2.6	5.8	2.3	N1<N2
Zooplankton WW. 0-600 m (mg m^{-3})	6.3	3.4	5.6	1.8	No difference
Micronekton (net) mg m^{-3})	3.4	3.0	7.1	6.8	
Sv EK60 0-600 m (dB)	-77.8	2.7	-77.7	2.6	No difference at 100%
Micronekton (SEAPODYM 0-600 m mg m^{-3})	4.3	1.2	4.3	0.9	No difference at 100%

1332
1333
1334

1335

1336 Table 3. Correlations between estimates of zooplankton biomass derived from each of the
1337 sampling methods deployed during the cruises. Grouped Nectalis1 and 2 Spearman's
1338 correlations and p-values between zooplankton dry and wet weight measurements (in
1339 mg m^{-3}) from net sampling and their acoustic proxies, S-ADCP Sv (in decibels, dB) and TAPS
1340 biovolume (in mg m^{-3}) for the averaged top 100 m and top 200 m. Statistics involving S-
1341 ADCP Sv is performed by calculating $\log_{10}$ of TAPS biovolume, zooplankton DW and WW.

Variables	Spearman's correlation coefficient		p-value	
	0-100 m	0-200 m	0-100 m	0-200 m
S-ADCP Sv vs. $\log_{10}$(TAPS biovolume)	0.58	0.64	7e-5*	7e-6*
S-ADCP Sv vs. $\log_{10}$(zoopl. dry weight from net)	0.53	0.66	6e-4*	1e-5*
S-ADCP Sv vs. $\log_{10}$(zoopl. wet weight from net)	0.44	0.36	5e-3*	0.03*
TAPS biovolume vs. zoopl. dry weight from net	0.52	0.61	9e-4*	6e-5*
TAPS biovolume vs. zoopl. wet weight from net	0.46	0.55	3e-3*	4e-4*

1342 * significant correlation at 5%

1343

1344

1345 Table 4. Correlations between estimates of micronekton biomasses. Grouped Nectalis1 and
1346 2 Spearman's correlations and significance between the four frequencies of S-ADCP Sv (dB)
1347 and the corresponding EK60 Sv (dB) averaged across 0-200m, and between estimates
1348 derived from $\log_{10}$ (SEAPODYM) and the corresponding 38 kHz EK60 Sv (dB) average across
1349 0-350 m. Statistics involving S-ADCP Sv is performed by calculating $\log_{10}$ of TAPS biovolume,
1350 zooplankton DW and WW.

1351

Variables	Range of Spearman's correlation coefficient	Percentage of significant correlations at α=0.05
S-ADCP Sv vs. 200 kHz EK60 Sv	0.83-0.90	100%
S-ADCP Sv vs. 120 kHz EK60 Sv	0.85-0.92	100%
S-ADCP Sv vs. 70 kHz EK60 Sv	0.87-0.96	100%
S-ADCP Sv vs. 38 kHz EK60 Sv	0.73-0.79	100%
Log_{10}(SEAPODYM) vs. 38 kHz EK60 Sv	0.66-0.80	100%

1352

1353

1354

Figures

Figure 1: Mean 1998-2007 primary production estimated from satellite (VGPM) in mgC m^{-2} d^{-1} (shading). Regions of ocean depth shallower than 200 m have been blocked out. Mean depth of the 1 µM nitrate isopleth (proxy for the nitracline depth) was extracted from CARS climatology (http://www.marine.csiro.au/~dunn/cars2009/) (Ridgway et al., 2002) in meters (contour lines) and mean 0-150 meter total geostrophic currents sourced from Kessler and Cravatte (2013) (vectors). The New Caledonia Exclusive Economic Zone is delineated by the white line.

Figure 2: Mean surface *in situ* (left column) and satellite-derived (right column) oceanographic conditions in the New Caledonian region during the cool season (Nectalis1 - 29 July to 16 August 2011): cruise track and station numbers with those sampled at night in bold red and those sampled during the day in regular black (top left); thermosalinograph sea-surface temperature in °C (SST) and salinity (SSS) (middle left); 0-150 m averaged currents in m s^{-1} (vectors) from the S-ADCP with blue and red arrows indicating eastward and westward currents respectively (bottom left); surface currents (vectors) from OSCAR (right column), scale identical to S-ADCP scale; MODIS-VGPM derived depth-integrated net primary production in mgC m^{-2} d^{-1} (top right); GHRSST satellite sea surface temperature in °C (top-middle right); sea level anomalies (SLA) referenced to the mean geoid in cm (bottom-middle right), letters indicate eddies identified in the text; eddy depiction index: Okubo-Weiß parameter (day^{-2}) (bottom right). The cruise track is plotted in black on the right column.

Figure 3: Mean surface *in situ* (left column) and satellite-derived (right column) oceanographic conditions in the New Caledonian region during the hot season (Nectalis2 - 26 November to 14 December 2011). See Figure 2 caption for details.

Figure 4. Biogeochemical parameters across 0-200 m along cruise tracks during the cool season (Nectalis1, left panel) and the hot season (Nectalis2, right panel), from CTD sensors and bottle water analyses. The x-axis labels denote station numbers. From top to bottom: temperature (°C), salinity, nitrate (NO_3 µM), phosphate (PO_4 µM), chlorophyll (mg m^{-3}) and

phytoplankton composition. The connected filled circles on the temperature and salinity panels represent the mixed layer depth, calculated as the depth at which the density equals the surface density + 0.03 kg m^{-3} (de Boyer Montégut et al., 2004). The connected filled diamonds on the chlorophyll panel represent the depth at which nitrate reaches 1 µM, a proxy for the nitracline depth. Phytoplankton composition is described as a percentage of picoplankton (< 3 µm, black), nanoplankton (3 µm to 10 µm, blue) and microplankton (> 10 µm, red) biomass; orange symbols represent the ratio of *Prochlorococcus* cells to total picoplankton cells (in % abundance); the dots represent the average value of the top 50 m and the crosses represent the average value of the 50-130 m layer.

Figure 5: Box plots of the distribution of *in situ* (In situ) primary production and satellite-derived (VGPM) primary production recorded at the points where *in situ* production measurements were performed (Sat.) and along the cruise track (Sat. full). Estimates are given for the cool (Nectalis1) and the hot season (Nectalis2). The boxplots denote mean values and 25% and 75% interquartiles (IQ25 and IQ75 respectively); the whiskers represent IQ25-1.5x(IQ75-IQ25) and IQ75+1.5x(IQ75-IQ25); dots represent outliers.

Figure 6: Day (plain line) and night (dashed line) 0-600 m mean vertical profiles of zooplankton wet weight (mg m^{-3}) and mean vertical profiles of 38kHz EK60 scattering volume (dB) during the cool season (Nectalis1, thick line) and the hot season (Nectalis2, thin line).

Figure 7: Estimates of zooplankton and micronekton biomass during the day (D) and night (N) during the cool season (Nectalis1, 1) and the hot season (Nectalis2, 2) using the different methods employed during the cruises. From left to right: distributions of mean S-ADCP Sv (dB) across 0-150 m, mean TAPS biovolume (mg m^{-3}) across 0-200 m, mean zooplankton dry weight (DW, mg m^{-3}) across 0-200 m, mean zooplankton wet weight (WW, mg m^{-3}) across 0-200 m, micronekton wet weight (mg m^{-3}) from cumulated net samplings at discrete depths between 14 and 540 m, mean 38 kHz EK60 Sv (dB) across 0-350 m, and corresponding depth-averaged mean (epi- and mesopelagic layers) of micronecton biomass estimates from the SEAPODYM model. The boxplots denote mean values and 25% and 75% interquartiles (IQ25 and IQ75 respectively); the whiskers represent IQ25-1.5x(IQ75-IQ25) and

IQ75+1.5x(IQ75-IQ25); dots represent outliers. Note that biomass estimates from SEAPODYM and EK 60, have been identically averaged over three euphotic depths (~350 m) and day/time periods (see text for further details).

Figure 8. Spatial distribution of the epi- and mesopelagic micronecton biomass (mg m^{-3}) estimated from SEAPODYM at the stations and periods of the cruises (top panels) and the corresponding observed 38 kHz Sv from the EK60 echosounder (bottom) during the cool season (Nectalis1, left panel) and the hot season (Nectalis2, right panel). The day/night signal was removed from the data (see text for details). For the sake of clarity the EK 60 Sv data were arbitrarily re-transformed into a linear scale by computing $10^{-Sv/100}$, but the unit by itself has no significance. The EK 60 data have been vertically averaged over the same depths as the micronekton model incorporated into SEAPODYM (3 euphotic layers ~350 m) and the data was resampled onto the model ¼° grid resolution.

Figure 9: Satellite primary production (VGPM in mgC m^{-2} day^{-1}) and euphotic layer currents from GLORYS (top panel). Averaged micronekton biomass (mg m^{-3}) estimated by SEAPODYM and averaged currents from GLORYS across the water column (0 – 1000m) (bottom panel). Cool season (Nectalis1, left panel), hot season (Nectalis2, right panel).

1429 **Figure 1**

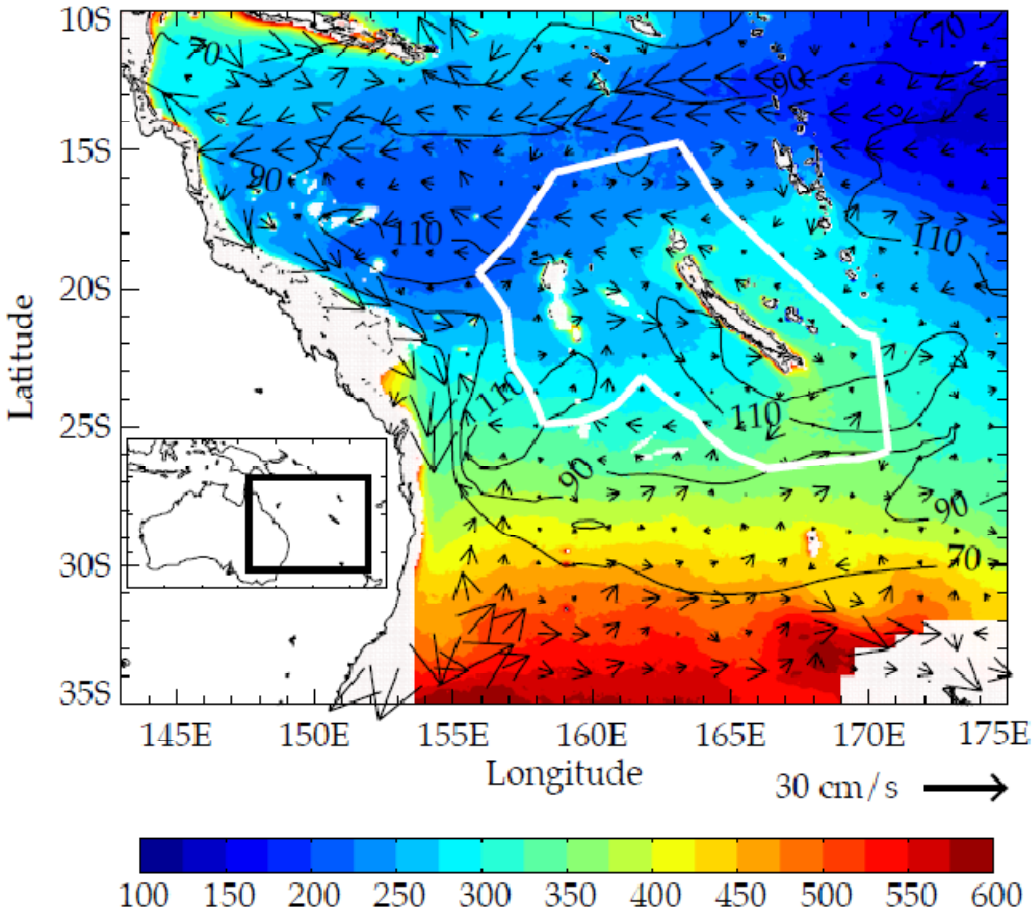

1430

1431

1432 **Figure 2**

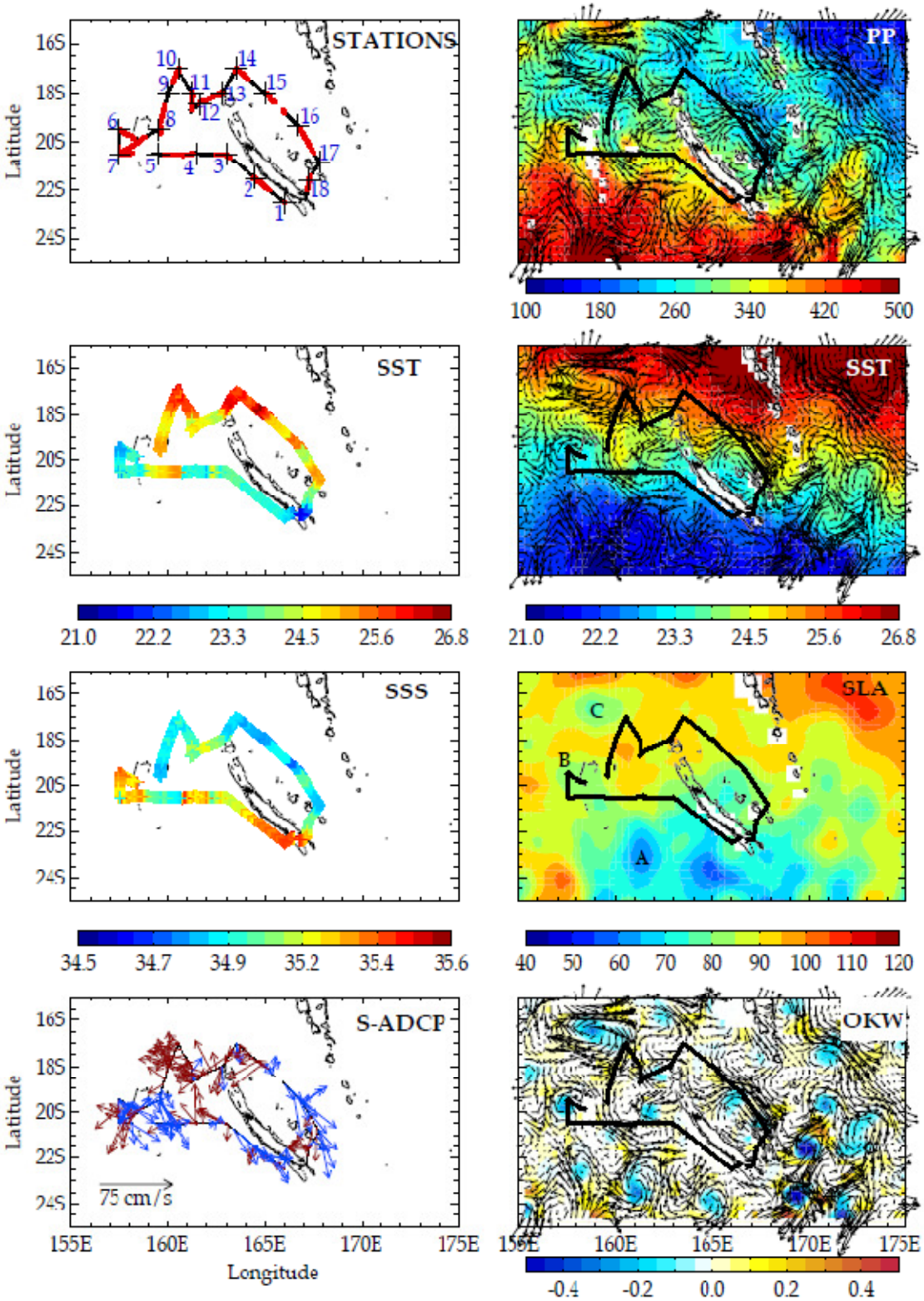

1433

1434

1435 **Figure 3**

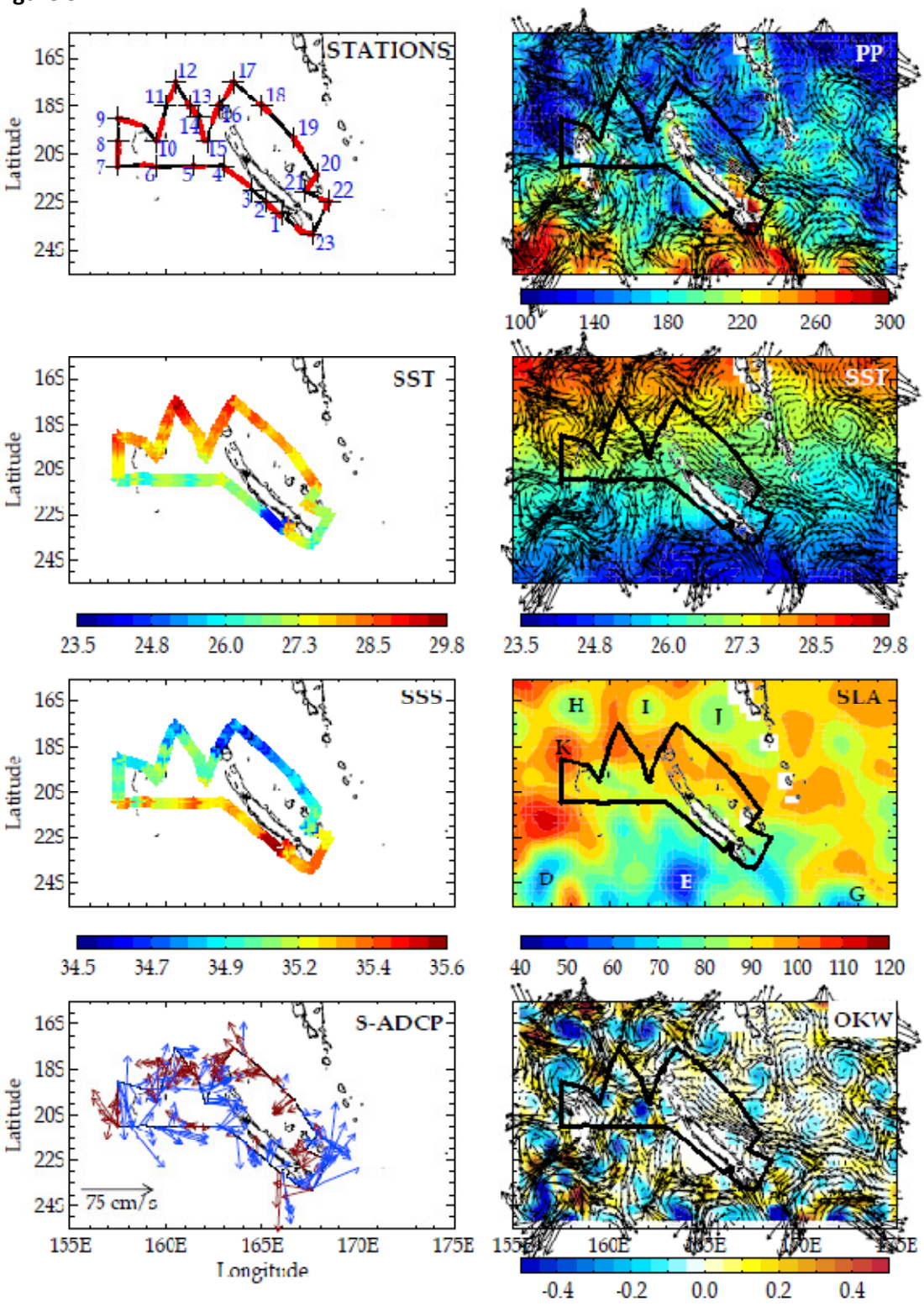

1436

1437 **Figure 4**

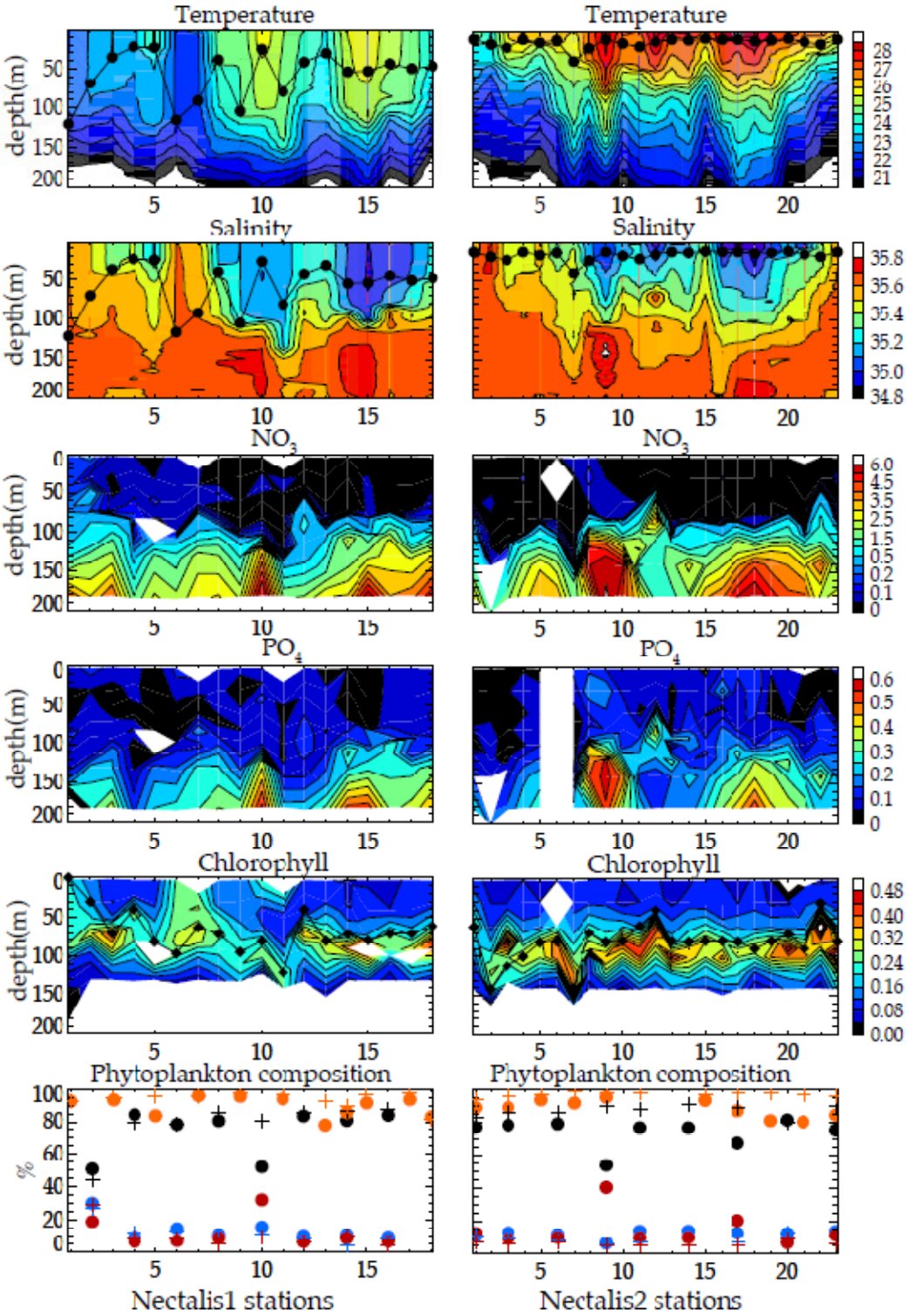

1438

1439

1440 **Figure 5**

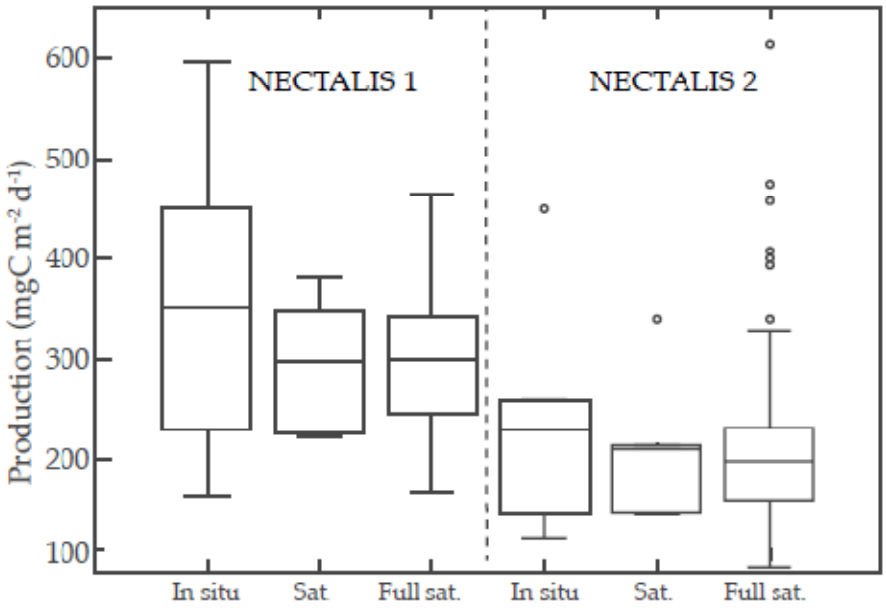

1441

1442

1443

1444 **Figure 6**

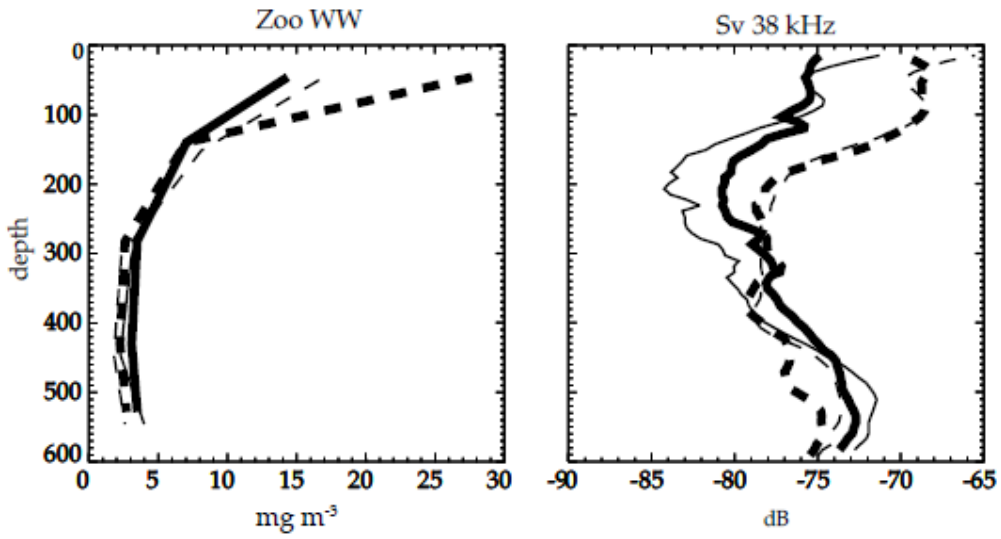

1445

1446

1447

1448 **Figure 7**

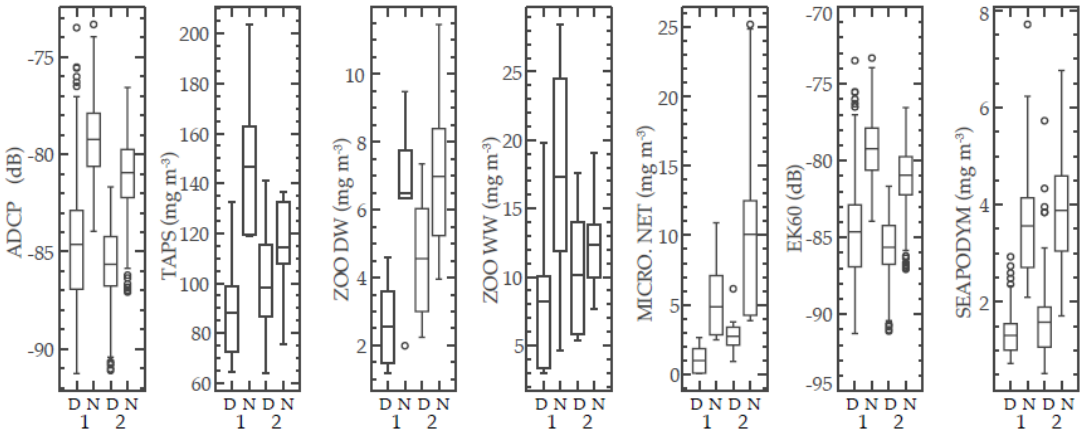

1449

1450

1451 **Figure 8**

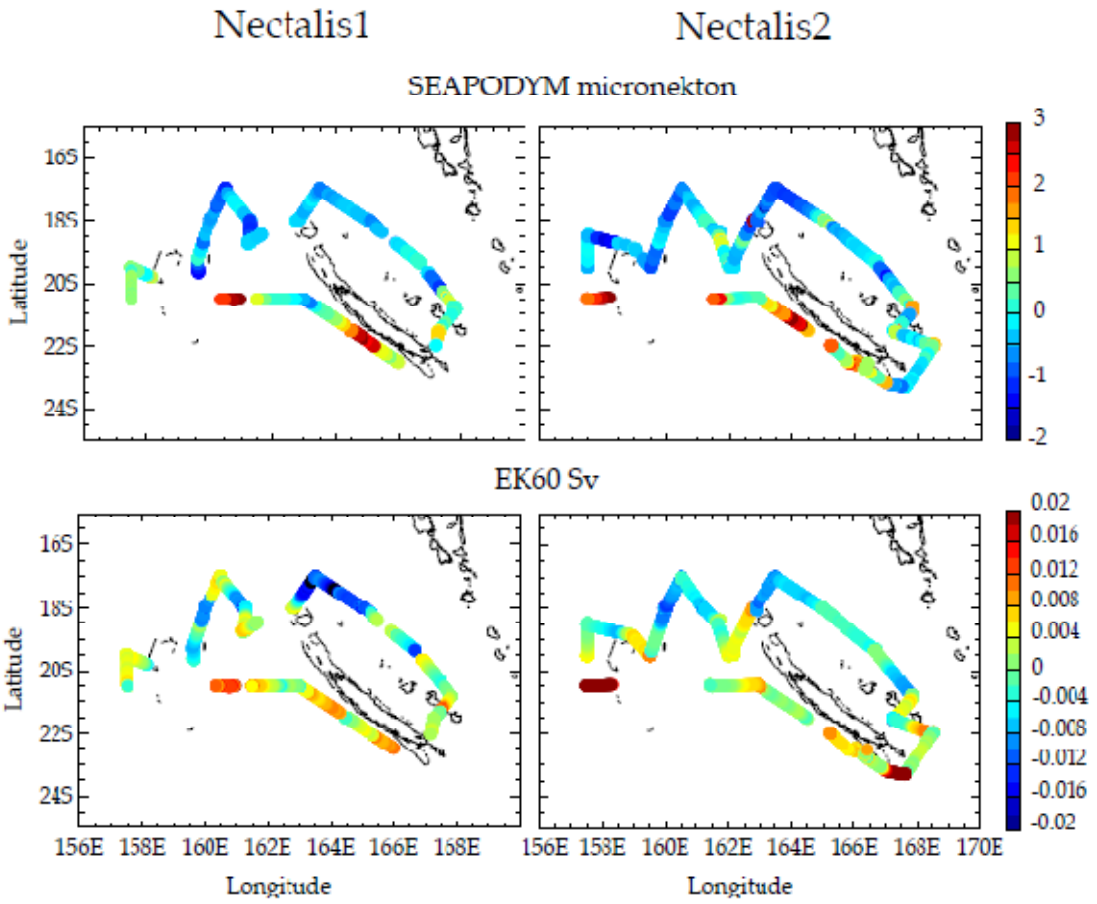

1452

1453

1454 **Figure 9**

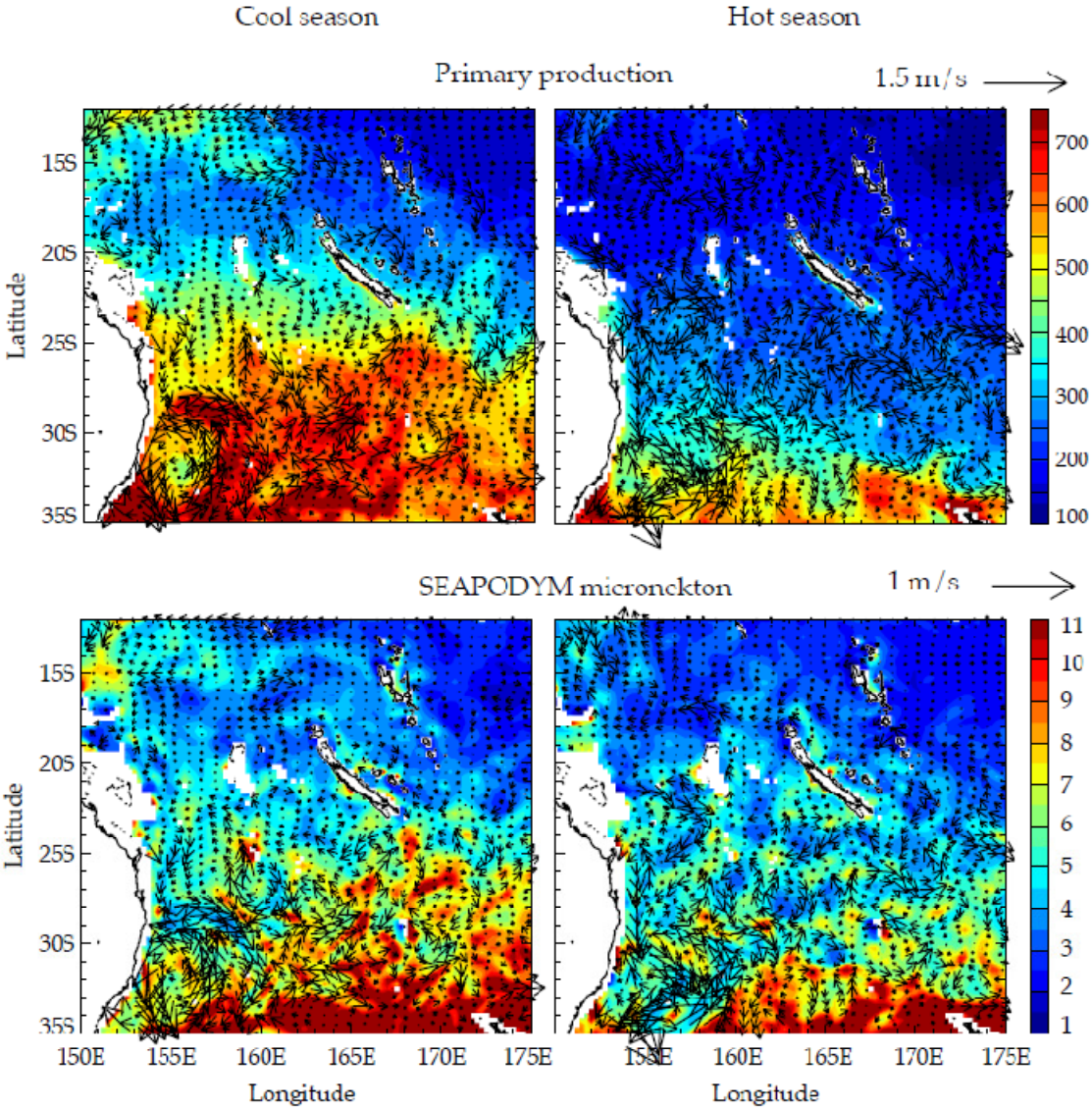

1455